JOURNAL OF PETROLOGY | VOLUME 49 | NUMBER 1 | PAGES 79–105 | 2008 | doi:10.1093/petrology/egm071

The Val Gabbro Plutonic Suite: A Sub-volcanic Intrusion Emplaced at the End of Flood Basalt Volcanism on the Kerguelen Archipelago

JAMES S. SCOATES[1]*, DOMINIQUE WEIS[1], MATTHIAS FRANSSENS[2], NADINE MATTIELLI[2], HEIDI ANNELL[1,3], FREDERICK A. FREY[4], KIRSTEN NICOLAYSEN[5] AND ANDRE GIRET[6]

[1]DEPARTMENT OF EARTH AND OCEAN SCIENCES, UNIVERSITY OF BRITISH COLUMBIA, VANCOUVER, BRITISH COLUMBIA, V6T-1Z4, CANADA

[2]DEPARTMENT OF EARTH AND ENVIRONMENTAL SCIENCES, UNIVERSITE LIBRE DE BRUXELLES CP160/02, AVENUE F. D. ROOSEVELT 50, B-1050, BRUSSELS, BELGIUM

[3]ANGLO AMERICAN EXPLORATION (CANADA) LTD., SUITE 800–700 WEST PENDER STREET, VANCOUVER, BRITISH COLUMBIA, V6C-1G8, CANADA

[4]DEPARTMENT OF EARTH, ATMOSPHERIC AND PLANETARY SCIENCES, MASSACHUSETTS INSTITUTE OF TECHNOLOGY, CAMBRIDGE, MA 02139, USA

[5]DEPARTMENT OF GEOLOGY, WHITMAN COLLEGE, WALLA WALLA, WA 99362, USA

[6]LABORATOIRE DE GEOLOGIE–PETROLOGIE, UNIVERSITE JEAN MONNET, CNRS-UMR 6524, SAINT-ETIENNE, FRANCE

RECEIVED JUNE 20, 2006; ACCEPTED OCTOBER 15, 2007
ADVANCE ACCESS PUBLICATION DECEMBER 1, 2007

The age, petrology, major and trace element geochemistry, and Sr–Nd–Hf–Pb isotopic geochemistry of basic and felsic rocks from the Val gabbro plutonic suite on the Kerguelen Archipelago, Southern Indian Ocean, are used to constrain the temporal and compositional relationships between sub-volcanic intrusions and flood basalt volcanism during the formation of a major oceanic island. The 4 km^2 Val gabbro plutonic suite was emplaced at 24·25 ± 0·15 Ma (U–Pb zircon) into 25 Ma volcanic rocks of the Southeast Province, locally producing a large zone of overlying basaltic breccia. Cumulate basic–ultrabasic rocks are the dominant lithology in the intrusion, with horizontally layered peridotites at the base of the exposed part of the intrusion, overlain by vertically layered, coarse-grained plagioclase-bearing peridotites, melagabbros and equigranular gabbros. The intrusion was formed by repeated injections of relatively crystal-rich and crystal-poor magmas into an open-system magma reservoir. Strong geochemical and isotopic similarities between the fine-grained marginal microgabbros and cross-cutting felsic rocks and the hosting mildly alkalic basalts and trachytes of the Southeast Province indicate that they were derived from similar alkalic basaltic parental magmas, which were dominated by the enriched component of the Kerguelen mantle plume source. At 25 Ma, the change from tholeiitic–transitional to mildly alkalic basalts marks the terminal stage of flood basalt volcanism on the Kerguelen Archipelago. This compositional change was associated with deeper melting within the Kerguelen plume source, lower extents of melting, a decrease in magma supply, and the emplacement of high-level intrusions such as the Val gabbro plutonic suite.

KEY WORDS: *Kerguelen Archipelago; Val gabbro plutonic suite; oceanic island; gabbros; sub-volcanic intrusion; alkalinity; Sr–Nd–Hf–Pb isotopes*

INTRODUCTION

The Kerguelen Archipelago in the Southern Indian Ocean contains some of the most extensive exposures of plutonic intrusions on an oceanic island. The first complete

*Corresponding author. Telephone: (604) 822-3667. Fax: (604) 822-6088. E-mail: jscoates@eos.ubc.ca

geological map of the Kerguelen Archipelago (Nougier, 1970) showed that plutonic rocks represent ~5% of the exposures. Subsequent detailed mapping and petrological studies focused mainly on describing the internal structure and petrology of the intrusive bodies (e.g. Nougier & Lameyre, 1973; Lameyre *et al.*, 1976; Giret *et al.*, 1980; Giret & Lameyre, 1984). In a reconnaissance isotopic study of plutonic rocks from the archipelago, Weis & Giret (1994) demonstrated that the intrusive rocks had broadly similar Sr, Nd, and Pb isotopic compositions to the relatively few volcanic rocks that had been analyzed. More recently, systematic studies of the volcanic sequences have been undertaken (e.g. Gautier *et al.*, 1990; Weis *et al.*, 1998; Yang *et al.*, 1998; Frey *et al.*, 2000, 2002; Doucet *et al.*, 2002) and now allow for better comparisons with the plutonic rocks. In this paper, we present the results of a detailed petrological, geochemical, geochronological, and Sr–Nd–Hf–Pb isotopic study of the Val gabbro plutonic suite in the Southeast Province of the Kerguelen Archipelago. Among the many intrusions on the archipelago, the Val gabbro plutonic suite was selected for study because of its importance in paleotectonic models of the Kerguelen Archipelago. Based on a K–Ar whole-rock age of 39 Ma and low total alkali contents for many of the coarse-grained basic rocks, it was considered to be a tholeiitic intrusion that represented the earliest hotspot-related magmatic products, when the archipelago was centred near or along the Southeast Indian Ridge (Giret & Lameyre, 1984; Giret & Beaux, 1984). This age is inconsistent with the results of recent Ar–Ar dating of basalts from across the archipelago, which has established a 5 Myr record of flood basalt volcanism in the interval from 24 to 29 Ma (Frey *et al.*, 2000; Nicolaysen *et al.*, 2000; Doucet *et al.*, 2002) when the Kerguelen Archipelago was in an intraplate setting. Establishing the precise age and parent magma composition of the Val gabbro plutonic suite on the Kerguelen Archipelago allows for a more detailed assessment of magmatic evolution on this major oceanic island and of the temporal relationship between subvolcanic intrusions and flood basalt volcanism related to the Kerguelen hotspot.

GEOLOGICAL SETTING OF THE KERGUELEN ARCHIPELAGO AND SOUTHEAST PROVINCE

The 6500 km^2 Kerguelen Archipelago, the emergent part of the Northern Kerguelen Plateau, is mainly composed of sub-horizontal basaltic lava flows (~85% of the exposed area) with the remaining area represented by plutonic rocks, Quaternary deposits, and glacial ice caps (Fig. 1). Based on recent Ar–Ar dating of basaltic whole-rocks and plagioclase separates, the major volcanic activity that formed the flood basalts currently exposed on the archipelago began at ~29 Ma and continued until 24–25 Ma (Nicolaysen *et al.*, 2000). Studies of the age and chemical stratigraphy of sections through the flood basalts show that the northern and central parts of the Kerguelen Archipelago, represented by the Bureau, Rabouillère, Fontaine, Ruches and Tourmente sections, are covered by 26–29 Ma tholeiitic–transitional basalt flows (Yang *et al.*, 1998; Doucet *et al.*, 2002; Frey *et al.*, 2002). In contrast, volcanic rocks from the eastern and southern parts of the archipelago, including the Courbet Peninsula (Crozier section) and the Southeast Province (Ravin du Charbon and Jaune sections) are characterized by 24–25 Ma mildly alkalic basalts and locally differentiated trachyandesites and trachytes (Weis *et al.*, 1993; Frey *et al.*, 2000; Damasceno *et al.*, 2002). Magmatic activity younger than the flood basalt volcanism on the Kerguelen Archipelago involved the emplacement of high-level alkaline intrusions within the flood basalts (see below) and the formation of the recent (2–0·1 Ma) basaltic to trachytic stratovolcano, Mont Ross (Weis *et al.*, 1998) (Fig. 1). The most recent eruption on the archipelago is represented by a 26 ± 3 ka (^{40}Ar/^{39}Ar sanidine) trachytic ignimbrite on the Rallier-du-Baty Peninsula (Gagnevin *et al.*, 2003).

Plutonic rocks are found throughout the archipelago (Fig. 1) and were the focus of much of the original work on the geology of the Kerguelen Archipelago, especially the 150 km^2 Rallier-du-Baty alkaline ring complex (Lameyre *et al.*, 1976; Dosso *et al.*, 1979; Giret *et al.*, 1980; Giret & Lameyre, 1984). Based on mapping and petrographic studies (Giret, 1983; Beaux, 1986), combined with conventional whole-rock K–Ar dates (J. M. Cantagrel, unpublished data) and whole-rock Rb–Sr isochron ages (Weis & Giret, 1994), the plutonic rocks were originally divided into three distinctive compositional series: (1) 39–24 Ma transitional plutonism, including the Val gabbro plutonic suite on the Jeanne d'Arc Peninsula of the Southeast Province (the focus of this study), the Monts Mamelles intrusion on the Courbet Peninsula, and the Anse du Jardin sill on the Loranchet Peninsula; (2) 26–13 Ma silica-undersaturated alkaline plutonism in the central and eastern parts of the archipelago, including the Société de Géographie, Monts Ballons and Montagnes Vertes intrusions; (3) 17–4 Ma silica-oversaturated alkaline plutonism, mainly located on the western part of the archipelago and including the Rallier-du-Baty, Ile de l'Ouest and Iles Nuageuses intrusions (Fig. 1).

The Southeast Province consists of the Jeanne d'Arc and Ronarc'h Peninsulas (Fig. 2a). Two distinct magmatic series occur within the Southeast Province (Leyrit, 1992; Weis *et al.*, 1993; Frey *et al.*, 2000) (Fig. 2a): (1) 25 Ma mildly alkalic basalts to trachytes that form the majority of the Jeanne d'Arc Peninsula and the lower elevations of the Ronarc'h Peninsula; these volcanic rocks were originally referred to as the Lower Miocene series, based on

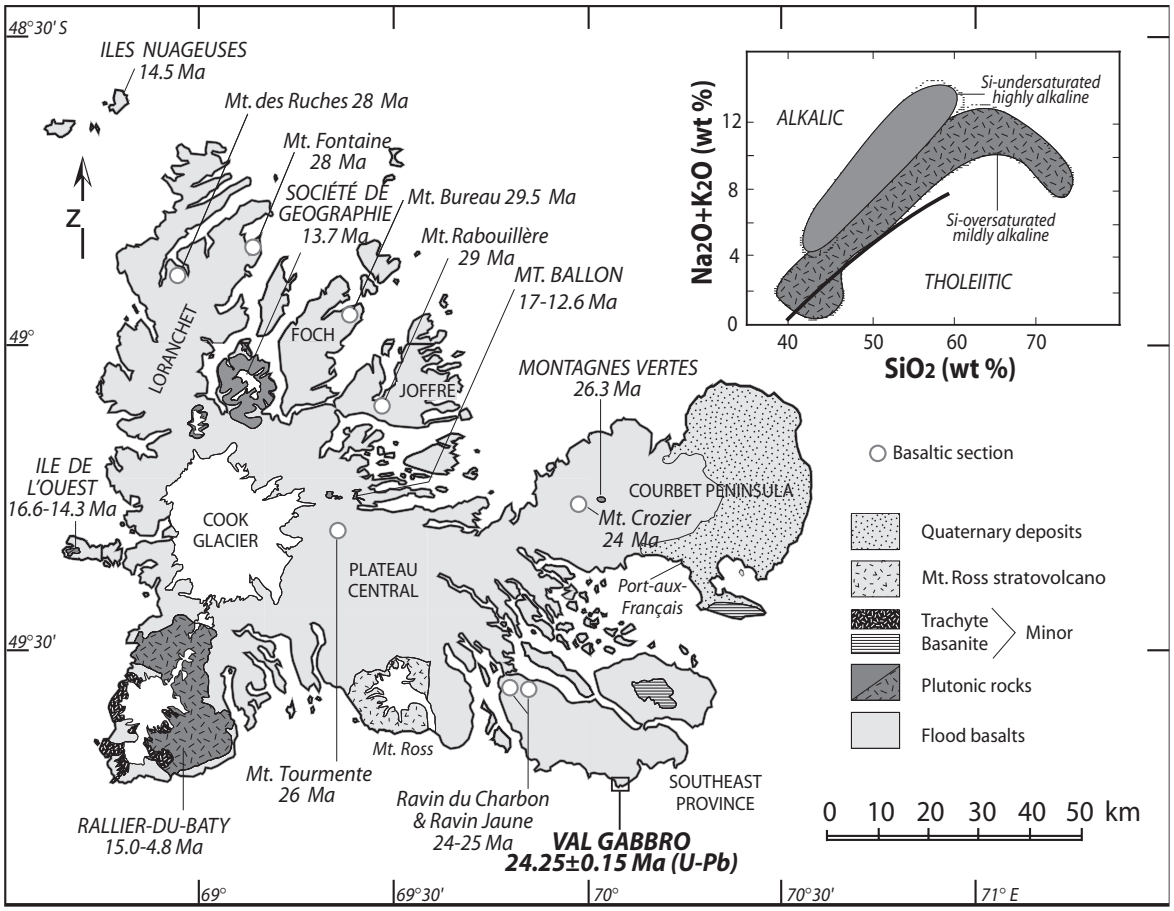

Fig. 1. Geological map of the Kerguelen Archipelago (after Nougier, 1970) showing the locations and ages of the main plutonic suites and studied basaltic sections. The Val gabbro plutonic suite is located in the southeastern corner of the Southeast Province and is labeled in bold italic capital letters. All other major intrusive suites on the archipelago are labeled with italic capital letters. The ages for the basaltic sections are all by the ^{40}Ar–^{39}Ar method and reported by Frey *et al.* (2000), Nicolaysen *et al.* (2000) and Doucet *et al.* (2002); the ages for the Mont Ross stratovolcano are by the K–Ar method reported by Weis *et al.* (1998). The ages for the plutonic rocks are from Dosso *et al.* (1979) (K–Ar method) and Weis & Giret (1994) (Rb–Sr isochron method), except for the U–Pb zircon age for the Val gabbro plutonic suite (this study). The inset shows a total alkalis–silica compilation diagram for mildly alkalic silica-oversaturated and alkalic silica-undersaturated plutonic suites on the Kerguelen Archipelago (Marot & Zimine, 1976; Giret, 1983; Beaux, 1986). The tholeiitic–alkalic boundary (bold line) is from MacDonald & Katsura (1964).

early K–Ar dates in the range 20–22 Ma (Nougier *et al.*, 1984), although more recent Ar–Ar dates of 25 Ma (Frey *et al.*, 2000) indicate that the Southeast Province volcanic rocks are Oligocene (the currently accepted age for the base of the Miocene is 23·03 Ma; Gradstein *et al.*, 2004); (2) 6–10 Ma silica-undersaturated rocks (basanites to phonolites) that occur predominantly as plugs, domes, needles and minor flows mostly on the Ronarc'h Peninsula, and are referred to as the Upper Miocene series. The Southeast Province volcanic rocks are intruded by several small gabbroic (Gaby Island, Vallée des Neiges and Val) and felsic—monzonitic to syenitic—(Mont Berlioz and Mont Rouge) plutonic suites (Leyrit, 1992). Based on the observed slopes to the lava flows and the abundance of dikes, Leyrit (1992) proposed the existence of at least two major eruptive centres, one just offshore from Gaby Island in the west and one offshore from the Val gabbro plutonic suite in the east (Fig. 2a). A +10 to +15 mgal Bouguer gravity anomaly extends across the southeastern part of the Jeanne d'Arc Peninsula and may be due to dense intrusive rocks at shallow depths related to the Val gabbro plutonic suite (Recq & Charvis, 1986).

GEOLOGY OF THE VAL GABBRO PLUTONIC SUITE

The 4 km^2 Val gabbro plutonic suite is located in the southeastern part of the Jeanne d'Arc Peninsula (Cap du Challenger) (Fig. 2). The outcrops are concentrated along steep slopes leading down to the ocean, an area that is extremely difficult to access, and are also found inland along a NW–SE-oriented valley (Fig. 2b). The principal

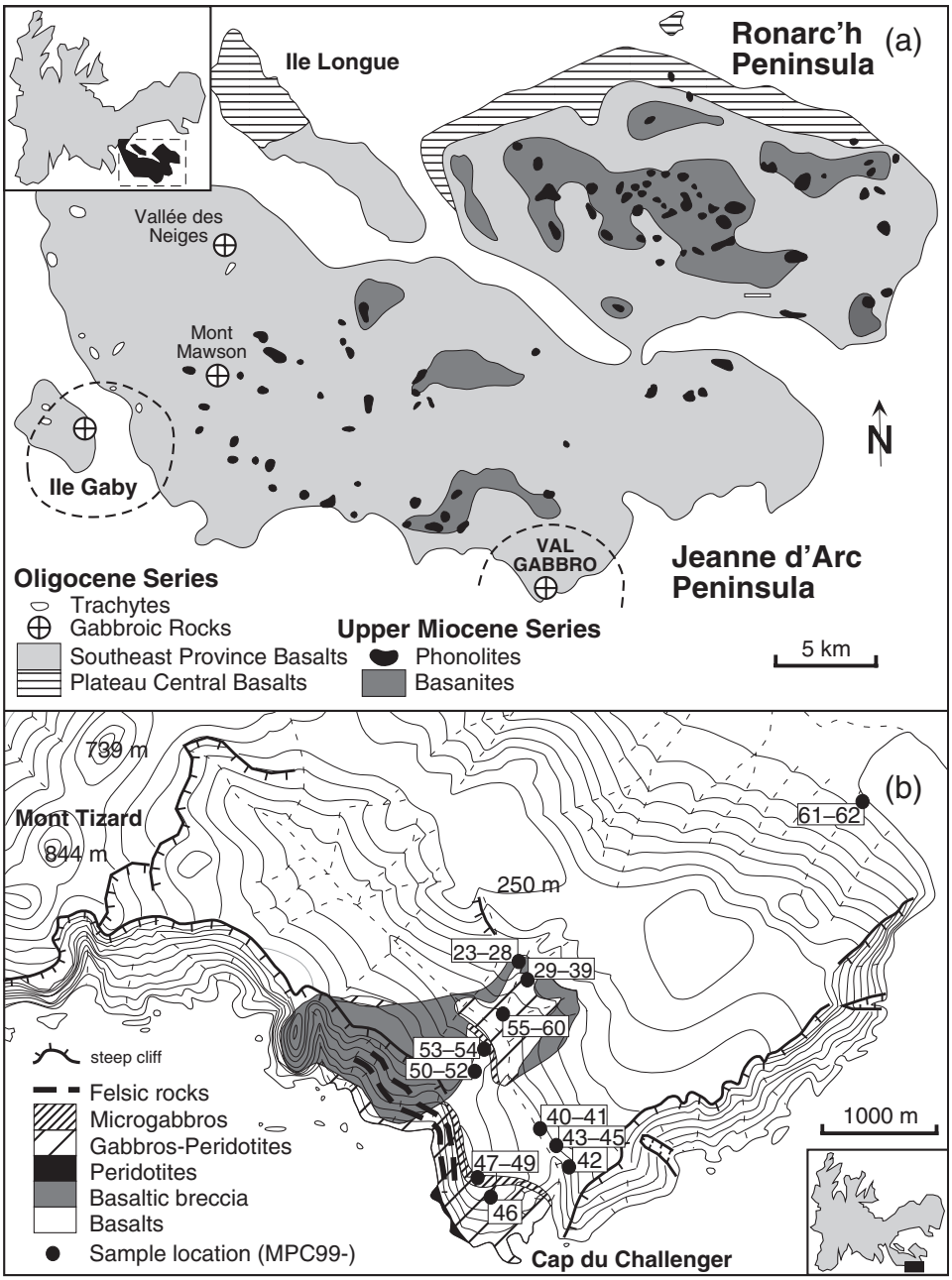

Fig. 2. Simplified geological maps showing the geological setting and lithological units of the Val gabbro plutonic suite. (a) Geological map of the Southeast Province, including the Jeanne d'Arc and Ronarc'h Peninsulas, after Leyrit (1992) and Frey *et al*. (2000). The Oligocene series rocks include volcanic rocks of the Southeast Province and Plateau Central, gabbroic intrusions, and trachytes. Volcanic rocks of the Southeast Province are predominantly 25 Ma mildly alkalic basalts with minor trachytic tuffs and flows. Occurrences of gabbroic intrusions include Gaby Island, Vallée des Neiges, Mont Mawson, and the Val gabbro plutonic suite. The two major eruptive areas for the Southeast Province lavas as described by Leyrit (1992) are indicated with bold dashed lines. Upper Miocene series rocks include 6–10 Ma basanites and phonolites, which are present as plugs, needles, and minor lava flows. (b) Geological map of the Val gabbro plutonic suite after Giret (1983). The topography, including stream beds (fine dashed lines), is shown; topographic contours are every 25 m. Sample locations are indicated (all sample numbers are preceded by MPC99-).

rock type within the exposed part of the Val gabbro plutonic suite is gabbro, which overlies peridotite. Peridotite forms the lower units of the plutonic suite near sea level at the base of the cliff and is characterized by horizontal igneous layering (Giret, 1983; Giret & Beaux, 1984). The peridotites are overlain by vertically layered basic–ultrabasic rocks consisting of coarse-grained melagabbro to peridotite and finer-grained gabbros (Fig. 3a).

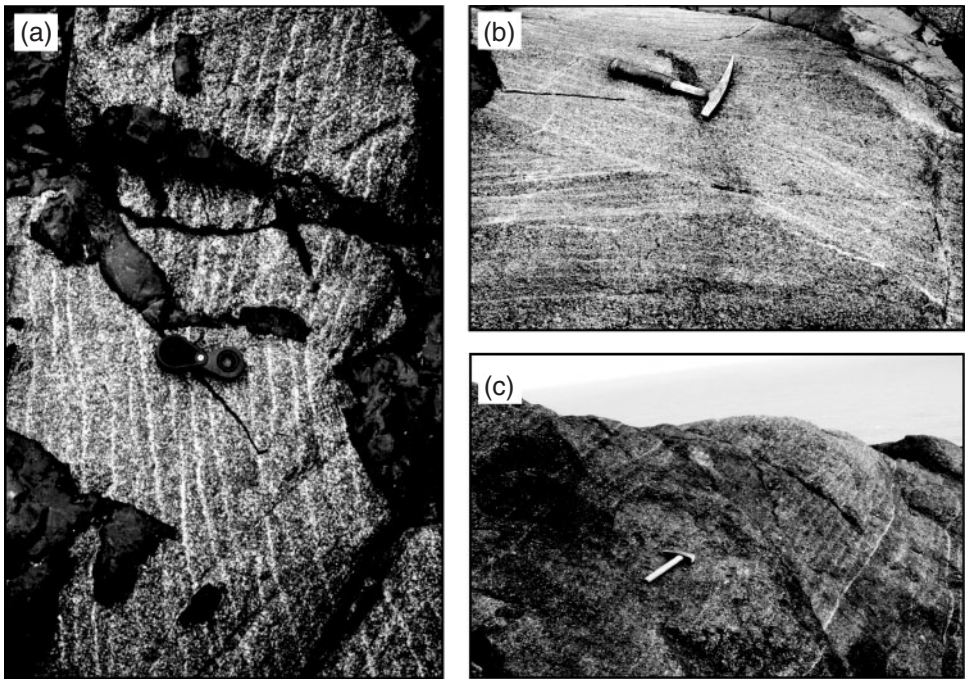

Fig. 3. Photographs showing typical layered structures in basic rocks of the Val gabbro plutonic suite. (a) Centimetre-scale modal layering where peridotite–melagabbro layers are separated by thin feldspathic layers. The layered intrusive rocks are cut by fine-grained basaltic dikes. Hand lens for scale. (b) Angular discontinuities in centimetre-scale modal layering from upper left to lower right of the photograph where two different orientations of layering are evident. Geological hammer for scale. (c) Repetitive centimetre-scale modal layering defined by thicker melagabbroic layers and thinner feldspathic layers with diffuse contacts. (Note the prominent white feldspathic layer in the right part of the photograph, which appears to represent the base of an angular discontinuity).

The centimetre-scale modal layering is predominantly vertical and oriented either north–south or east–west, parallel to the orientations of fractures in the host basalts. Angular discontinuities are commonly observed in the layered gabbros of the Val gabbro plutonic suite (Fig. 3b). Very fine-grained gabbros (<1 mm grain sizes), referred to as microgabbros in this study, occur locally along the contacts between the host basalts and the layered gabbros, and probably represent rapidly cooled or chilled margins to the Val gabbro plutonic suite. Intensely brecciated basalt overlies the layered gabbros in the northwestern part of the intrusion (Fig. 2b), which led Giret & Beaux (1984) to propose that the breccias represent a roof zone to the intrusion. The gabbros and adjacent basaltic breccia to the NW are cut by rare, irregular, quartz-bearing felsic dikes (shown in schematic form in Fig. 2b as thick dashed lines), which are typically sub-vertical and <10 cm thick. Two larger felsic dikes (~1 m thick) are observed in the cliff-face leading down to the ocean and appear to extend below sea level. Finally, the intrusive rocks of the Val gabbro plutonic suite are cut by numerous fine-grained basic dikes (Fig. 3a), which typically have a sub-vertical orientation. These dikes probably represent the feeder system for overlying lava flows that were erupted following emplacement of the intrusion.

PETROLOGY AND MINERAL CHEMISTRY OF THE VAL GABBRO PLUTONIC SUITE

The results of a petrological and geochemical study of 17 samples from the Val gabbro plutonic suite were reported by Giret (1983) and Giret & Beaux (1984). A new study was initiated because of (1) the possibility that the intrusion may represent part of a major eruptive centre for basaltic to trachytic lava flows of the Southeast Province (Leyrit, 1992), (2) the availability of additional geochemistry for volcanic rocks of the Southeast Province (Frey *et al.*, 2000) for comparison with the intrusive rocks, and (3) the existence in the literature of a 39 Ma K–Ar age for a gabbroic sample, a date that is inconsistent with recent $^{40}Ar/^{39}Ar$ whole-rock ages for basaltic rocks from across the archipelago (e.g. Nicolaysen *et al.*, 2000). A total of 40 new samples from the Val gabbro plutonic suite were collected during the French CartoKer mapping campaign on the Kerguelen Archipelago in February 1999. Twenty-seven samples were collected directly from outcrops and the remaining 13 samples (MPC99-40, 41, 43, 44, 45, 50, 53, 55–60) were collected from large fresh blocks adjacent to outcrops or from rockfalls along streambeds; sample locations for the new series are shown in Fig. 2b. Both the new

samples and the previously collected samples can be divided into three main groups: (1) basic to ultrabasic intrusive rocks, including coarse-grained peridotites and melagabbros, equigranular gabbros, microgabbros, and subophitic microgabbros; (2) felsic intrusive rocks, consisting mostly of very fine-grained monzonites and quartz monzonites in this study, with minor syenites and granites (Giret, 1983); (3) volcanic rocks, representing the hosting mildly alkalic basalts of the Southeast Province. It should be noted that no samples are available from the layered peridotites along the base of the cliff-face (Fig. 2) or from the late basic dikes that cut the intrusive rocks.

Representative electron microprobe analyses of olivine and clinopyroxene from the earlier series of samples (AG77) have been reported by Giret (1983); however, there were no analyses of these minerals for the coarse-grained peridotites and melagabbros as they were not sampled in the earlier study. In this study, electron microprobe analyses of olivine and clinopyroxene were acquired on a fully automated Cameca SX-50 microprobe at the University of British Columbia, operating in wavelength-dispersion mode, with the following operating conditions: excitation voltage 15 kV; beam current 20 nA; beam diameter 5 μm; peak count-time 20 s; background count-time 10 s. Data reduction was done with the 'PAP' $\phi(\rho Z)$ method (Pouchou & Pichoir, 1991) using natural standards. Compositions were typically determined from three grains of each mineral per sample with three point analyses per grain (one analysis in the core of the crystal, one from the crystal rim, and one additional analysis at an intermediate distance between the core and rim). The complete mineral chemistry results (78 olivine and 89 clinopyroxene analyses) are available in an Electronic Appendix, which can be downloaded at http://www.petrology.oxfordjournals.org/. All analyses reported are consistent with mineral stoichiometry.

Basic to ultrabasic intrusive rocks

The coarse-grained intrusive rocks are plagioclase-bearing peridotites to olivine melagabbros, subsequently referred to as peridotites in this study for simplicity, and contain abundant euhedral olivine and clinopyroxene (60–90 vol. %) ranging in size from 1 mm to >1 cm (Fig. 4). The peridotites are subdivided into two main rock types: wehrlites and olivine clinopyroxenites. The interstices between the larger grains contain discrete anhedral plagioclase and/or pyroxene grains (>1 mm grain sizes) in the wehrlites (samples MPC99-32, 34, 38, 39), or a fine-grained gabbroic matrix (<0·1 mm grain sizes) in the olivine clinopyroxenites (samples MPC99-35, 36, 40, 41, 43). Olivine core compositions are in the range of $Fo_{76–86}$ in the wehrlites and $Fo_{68–84}$ in the olivine clinopyroxenites; many of the olivine clinopyroxenites contain olivine that is distinctly more Fe-rich than in the wehrlites (Fig. 5a). Normal zoning ($\Delta Fo_{core–rim} = 6–10$ mol %) is characteristic of more than half of the analyzed grains, with the remaining grains showing only minor to no zonation. Nickel contents of olivine cores range from 0·31 wt % NiO at $Fo_{84·3}$ in the wehrlites to 0·1 wt % NiO at $Fo_{70·9}$ in the olivine clinopyroxenites. Oscillatory zonation is characteristic of clinopyroxene in all olivine clinopyroxenites and clinopyroxene-rich melagabbros. Clinopyroxene core compositions show a limited range of Fe/Mg and plot within the restricted field for clinopyroxene phenocrysts from mildly alkalic basalts from the Crozier section on the Courbet Peninsula (Damasceno *et al.*, 2002) and especially from the high-MgO basalts and picrites sampled as cobbles from glacial moraines on the archipelago (Doucet *et al.*, 2005) (Fig. 5b). Alumina contents in clinopyroxene range from 1·1 to 4·6 wt % Al_2O_3. Sample MPC99-43 is distinctive because of the relatively low abundance of mafic minerals (40 vol. %), which are predominantly large (up to 1 cm diameter) euhedral clinopyroxene crystals with strong, oscillatory zonation. Olivine and clinopyroxene are interpreted to be cumulus minerals in the peridotites based on their high modal abundances, euhedral grain shapes, and Mg-rich mineral compositions. There is little evidence for textural equilibrium (e.g. straight grain boundary contacts, 120° triple junctions) between olivine and clinopyroxene grains, suggesting that cooling rates were sufficiently high at the level of emplacement of the Val gabbro to prevent subsolidus re-equilibration.

The equigranular gabbros (MPC99-30, 31, 44, 45, 46, 58, 59 and 60) are dominated by highly variable proportions of millimetre-sized subhedral plagioclase and euhedral to equigranular, zoned clinopyroxene crystals (Fig. 4). There is no preferred alignment to the orientation of the plagioclase laths (width/length ~1/3). Samples MPC99-45 and 59 are distinctive from the other equigranular gabbros; sample MPC99-45 contains abundant plagioclase (83% CIPW normative content) and sample MPC99-59 contains abundant Fe–Ti oxides. Olivine is typically a minor phase, or absent, except in MPC99-46, where fresh and/or altered euhedral olivine grains occupy up to 20 vol. % of the sample. Interstitial biotite forms 5 and 15 vol. % of samples MPC99-45 and 46, respectively. Alteration is minor in most samples, except MPC99-30, which contains ~10 vol. % chlorite.

The microgabbros (MPC99-23, 28, 51, 52 and 54) and the subophitic microgabbros (MPC99-24, 25 and 26) are the finest-grained basic rocks in the Val gabbro plutonic suite (Fig. 4). In the microgabbros, both plagioclase and clinopyroxene are present as uniformly fine-grained crystals (<1 mm). Sample MPC99-52 is distinctive in that it contains a fine-grained matrix with abundant (~15 vol. %) coarser-grained (up to 6 mm) clinopyroxene and olivine crystals (Fig. 4), which vary from euhedral to irregular and resorbed in shape and which resemble the mafic crystals in the peridotites and melagabbros.

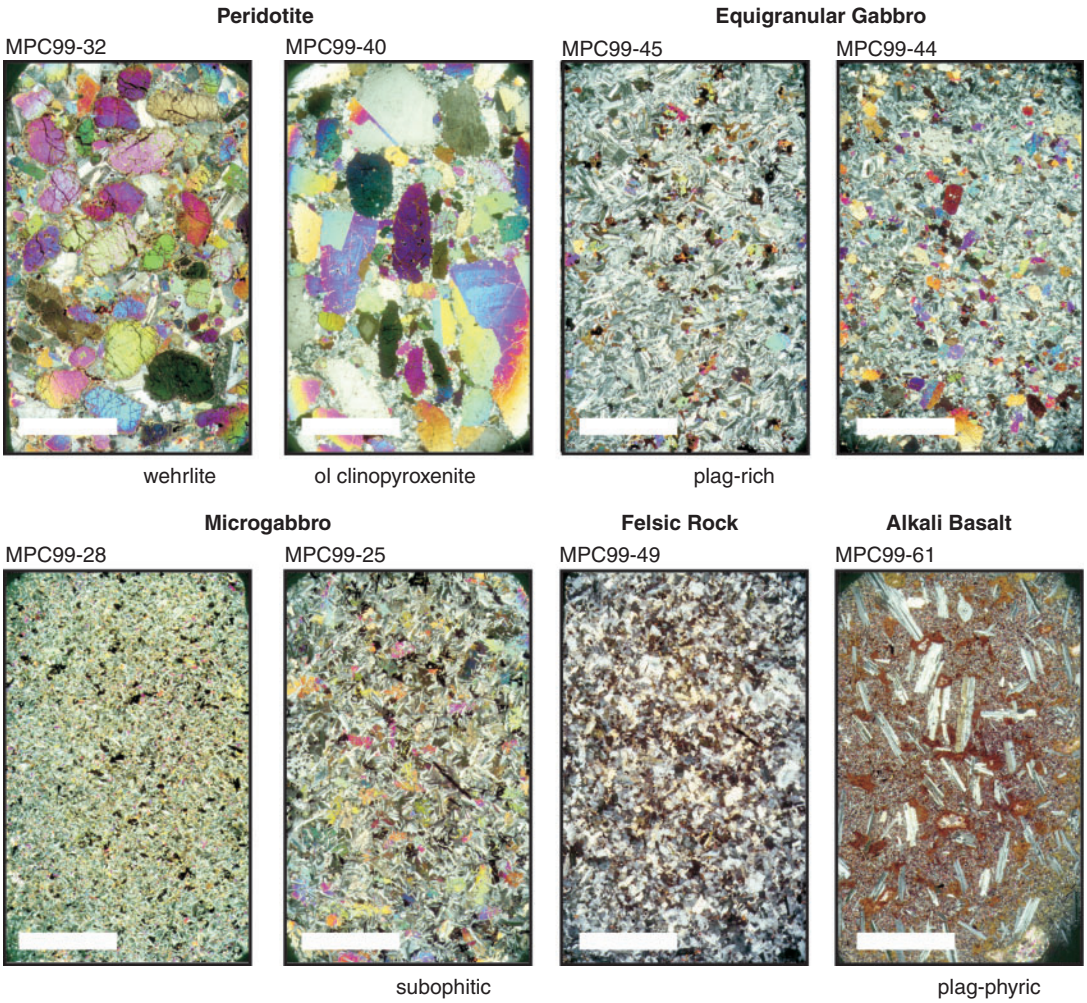

Fig. 4. Full thin-section photomicrographs (25 mm × 48 mm; crossed polarizers) of samples representative of the rock types observed in the Val gabbro plutonic suite. The upper row shows examples of cumulate rocks, including olivine-rich (MPC99-32) and clinopyroxene-rich (MPC99-40) coarse-grained peridotites and the finer-grained equigranular gabbros (MPC99-44 and 45). The lower row shows examples of non-cumulate rocks, including microgabbro (MPC99-28), subophitic microgabbro (MPC99-25), fine-grained monzonite (MPC99-49), and a plagioclase-phyric mildly alkalic basalt (MPC99-61), typical of the hosting volcanic rocks of the Southeast Province. The scale bars represent 1 cm.

The subophitic microgabbros contain 60–80 vol. % plagioclase, typically elongate (width/length ~1/10), millimetre-sized and zoned, and 15–30 vol. % clinopyroxene, which is pink in plane-polarized light (titanaugite), weakly zoned to unzoned, and poikilitic. Minor amounts (<5 vol. %) of interstitial quartz and calcite occur in each of the examined samples and both minerals contain abundant acicular apatite and locally euhedral zircon grains.

Felsic intrusive rocks

The felsic intrusive rocks, including samples MPC99-47, 48, 49, 50, 53A (53a/A, 53 b/A, 53c/A), 56 and 57, are monzonites to quartz monzonites with grain sizes <1 mm. Plagioclase is commonly strongly zoned with altered sodic rims. Euhedral to anhedral alkali feldspar crystals are locally microperthitic and variably altered to fine-grained sericite. Green to brown amphibole is present in most samples as well as small clots of titanomagnetite and clinopyroxene that are interpreted to represent amphibole breakdown products during late-stage oxidation, a feature typical of plutonic rocks on the Kerguelen Archipelago (Giret *et al.*, 1980). Minor clinopyroxene, fayalitic olivine, and quartz are also present. Fe–Ti oxides, predominantly ilmenite, occur in most samples. Euhedral zircon and needles of apatite are typically present as accessory minerals. Sample MPC99-47 is notably more feldspar-rich than the other samples and does not contain quartz, and the feldspar in sample MPC99-56 is more extensively altered compared with the other felsic rocks. Sample MPC99-56 also contains abundant 1–3 mm diameter rounded clots of

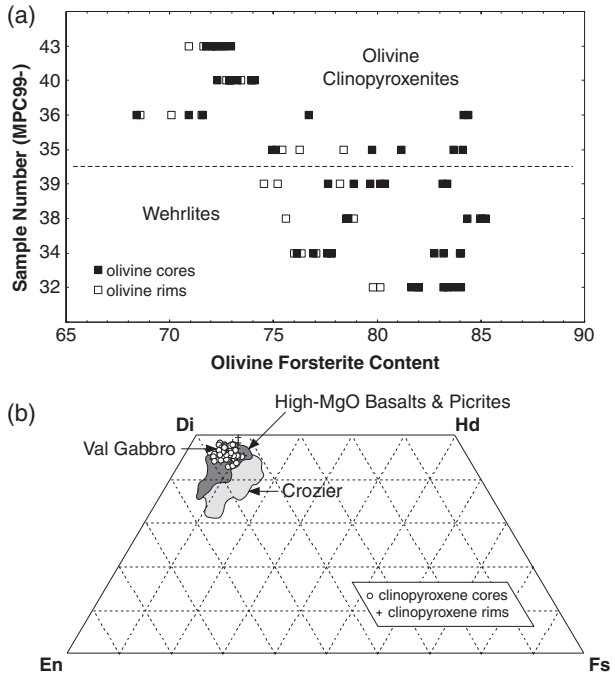

Fig. 5. Variations in olivine and clinopyroxene compositions from coarse-grained peridotitic cumulate rocks from the Val gabbro plutonic suite. (a) Range of olivine forsterite contents with core compositions indicated by filled squares and rim compositions by open squares. (b) Clinopyroxene compositions projected into the Di–Hd–En–Fs pyroxene quadrilateral. The limited range of compositions is similar to that observed in mildly alkalic high-MgO basalts and picrites from across the eastern part of the Kerguelen Archipelago (Doucet *et al.*, 2005) and in mildly alkalic basalts from the Crozier section on the Courbet Peninsula (Damasceno *et al.*, 2002).

finer-grained igneous inclusions that are significantly more oxide- and plagioclase-rich than the matrix of the sample.

Volcanic rocks

Five volcanic rocks (MPC99-42, 53a/B, 53c/B, 61 and 62) representative of the host rocks to the Val gabbro intrusive complex were also sampled to investigate possible thermal and/or alteration effects related to emplacement of the gabbroic rocks and to compare with volcanic rocks from elsewhere in the Southeast Province. Local hornfelsing (1 cm thickness) of the host basalt is observed only in sample MPC99-53, which contains plagioclase-phyric alkali basalt in contact with the plutonic rocks (i.e. the contact runs through the sample). Sample MPC99-42 is a weakly plagioclase-phyric alkali basalt (<5 vol. % phenocrysts). Samples MPC99-61 and 62, taken 3 km to the NE of the exposed plutonic rocks (Fig. 2b), are strongly plagioclase-phyric alkali basalts (~15 vol. % phenocrysts) with large tabular plagioclase phenocrysts up to 1 cm in length (Fig. 4), which is typical of flows observed throughout the Southeast Province (Weis *et al.*, 1993; Frey *et al.*, 2000).

AGE OF THE VAL GABBRO PLUTONIC SUITE

The previously reported ages for the Val gabbro plutonic suite are 39 ± 3 Ma for a gabbroic rock (sample AG78-04) and $27{\cdot}4 \pm 0{\cdot}8$ Ma for a felsic dike (sample AG78-31) [K–Ar whole-rocks; J. M. Cantagrel, unpublished data, cited by Giret *et al.* (1981) and Giret & Lameyre (1984)]. The age of 39 Ma for the gabbroic rock is inconsistent with the structural setting of the Val gabbro plutonic suite, which is intrusive into the alkalic basaltic lava flows that envelop it, based on the following observations: (1) massive and/or vertically layered gabbroic rocks cross-cut the subhorizontal lava flows around the intrusion; (2) angular fragments of the enclosing alkalic basalts are found within the gabbros; (3) intensely brecciated basalt is found above and between the two main occurrences of gabbro (Fig. 2b). The first reported ages for basalts from the Southeast Province were $21{\cdot}9 \pm 0{\cdot}5$ Ma (K34: Arènes, Jeanne d'Arc) and $20{\cdot}0 \pm 0{\cdot}6$ Ma (K138: Calanque, Ronarc'h) obtained from whole-rocks by the K–Ar method (Nougier *et al.*, 1984). However, as noted by Nicolaysen *et al.* (2000), all existing whole-rock K–Ar ages from Kerguelen basalts and gabbros should be regarded with caution, as eruption ages inferred by the K–Ar method may be erroneous because of the effects of thermal resetting or low-temperature alteration. New $^{40}Ar/^{39}Ar$ ages (leached whole-rocks) for four volcanic rocks from the Southeast Province have been reported by Frey *et al.* (2000). The samples are from near Port Jeanne d'Arc on the NW corner of the Jeanne d'Arc Peninsula, including two samples from the Ravin du Charbon section (ARC731: $24{\cdot}85 \pm 0{\cdot}17$ Ma; ARC573: $25{\cdot}18 \pm 0{\cdot}36$ Ma) and two samples from the Ravin Jaune section (ARC686: $24{\cdot}99 \pm 0{\cdot}16$ Ma; ARC678: $24{\cdot}83 \pm 0{\cdot}16$ Ma) (all ages are inverse isochron ages where the error quoted is 2σ). That this average age of ~25 Ma is equally valid for other volcanic rocks from the Southeast Province is corroborated by the Rb–Sr isochron age of ~25 Ma reported for alkali basalts and trachytes by Weis *et al.* (1993).

In light of the structural evidence for an intrusive origin for the Val gabbro plutonic suite and the coherent age of ~25 Ma for volcanic rocks of the Southeast Province, we have (1) re-examined the original gabbroic sample that was dated (AG78-04) to assess the possible role of alteration on K–Ar systematics, and (2) determined the U–Pb ages of separated zircon and baddeleyite fractions from a subophitic gabbro (MPC99-24) from the intrusion. Sample AG78-04 is highly altered with abundant secondary chlorite, sericite and zeolites; it also contains significantly less K_2O (0·16 wt %; Giret, 1983) than equivalent rocks (equigranular gabbros) analyzed in this study (average K_2O is 0·85 wt %). This confirms that alteration has resulted in significant K loss and thus the previously reported K–Ar date for this sample should not be

Table 1: U–Pb data from zircon and baddeleyite fractions separated from sample MPC99-24 (subophitic microgabbro)

Sample[1]	Wt (mg)	U (ppm)	Pb (ppm)[2]	$^{206}Pb/^{204}Pb$ (meas.)[3]	Common Pb (pg)	% ^{208}Pb[2]	$^{206}Pb/^{238}U$[4] (±% 1σ)	$^{207}Pb/^{235}U$[4] (±% 1σ)	$^{207}Pb/^{206}Pb$[4] (±% 1σ)	$^{206}Pb/^{238}U$ age (Ma; ±% 2σ)	$^{207}Pb/^{235}U$ age (Ma; ±% 2σ)
B1: N10, <44	0·010	271	1·0	133	5	9·3	0·00371(0·38)	0·02391(3·75)	0·04676(3·57)	23·86(0·18)	23·99(1·78)
Z1: N10, <62	0·030	1195	6·0	449	19	32·2	0·00377(0·20)	0·02438(0·58)	0·04686(0·48)	24·28(0·10)	24·45(0·28)
Z2: N10, <62	0·032	1171	6·2	358	25	35·4	0·00376(0·18)	0·02419(0·64)	0·04666(0·53)	24·19(0·09)	24·27(0·31)

[1]N10, non-magnetic at 10° side slope on Frantz magnetic separator; grain size given in microns; B, baddeleyite; Z, zircon.
[2]Radiogenic Pb; corrected for blank, initial common Pb, and spike.
[3]Corrected for spike and fractionation.
[4]Corrected for blank Pb and U, and common Pb.

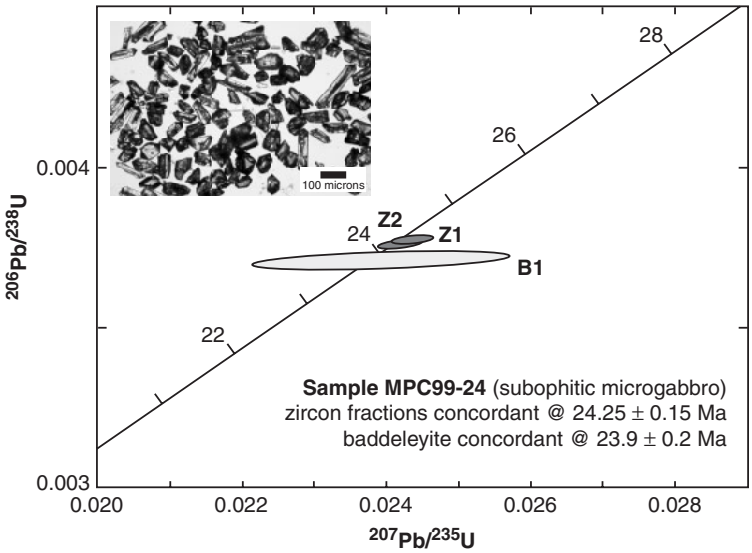

Fig. 6. U–Pb geochronological results from sample MPC99-24 (subophitic microgabbro). The concordia plot shows the U–Pb data from the two analyzed zircon fractions (Z1 and Z2) and the baddeleyite fraction (B1); each ellipse represents the result of the analysis of a single fraction. The inset is a photomicrograph showing the range in size and morphology of zircon grains from MPC99-24. Individual fractions of clear, inclusion-free zircon grains were picked from this bulk separate for dating.

considered geologically meaningful. Sample MPC99-24, a subophitic microgabbro from this study, contains microscopically visible euhedral zircon within interstitial quartz–carbonate patches. Zircon and baddeleyite were separated from a 3 kg split of the original sample using conventional crushing, grinding, Wilfley table, heavy liquids and Frantz magnetic separator techniques. The separated zircon grains were small (most <100 μm) and showed a range of aspect ratios from stubby, nearly equant grains to slender, high-aspect ratio (5:1) grains. Nearly all of the zircon grains were characterized by the presence of fluid inclusions. The separated zircon was split into two fractions for dissolution and analysis. About 10 grains, mostly fragments, of very fine-grained baddeleyite (<10 μm) were also present and all of this was analyzed as a single fraction. U–Pb isotopic analyses were carried out at the Pacific Centre for Isotopic and Geochemical Research at the University of British Columbia. The method for zircon and baddeleyite grain selection, dissolution, geochemical preparation, and mass spectrometry has been described by Mortensen *et al.* (1995). Procedural blanks for Pb and U were 2 and 1 pg, respectively. Table 1 contains all U–Pb results from this study and U–Pb data are plotted on a conventional U–Pb concordia plot in Fig. 6. Errors attached to single analyses were calculated using the numerical error propagation method of Roddick (1987) and decay constants used are those recommended by Steiger & Jäger (1977). Compositions for initial common Pb were taken from the model of Stacey & Kramer (1975). The errors on the ages are given at the 2σ level. U–Pb data from the two zircon fractions are concordant and yield a total range of $^{206}Pb/^{238}U$ ages of 24·25 ± 0·15 Ma,

which is interpreted as the age of crystallization of the subophitic microgabbro and thus of the Val gabbro plutonic suite. The U–Pb data from the single baddeleyite fraction are also concordant and the $^{206}Pb/^{238}U$ age is $23{\cdot}9 \pm 0{\cdot}2$ Ma. The relatively high error in $^{207}Pb/^{235}U$ for the baddeleyite fraction is due to the very low Pb concentration (Table 1) such that the blank correction has an impact on the calculated age. The U–Pb baddeleyite age is interpreted as a minimum age of crystallization and may reflect minor post-crystallization Pb loss.

WHOLE-ROCK SAMPLE PREPARATION AND GEOCHEMICAL ANALYTICAL TECHNIQUES

A total of 36 samples (23 basic and ultrabasic rocks, eight felsic rocks and five volcanic rocks) were prepared for geochemical analyses (sample locations are given in the Appendix). All weathered surfaces were sawn off and all fresh surfaces were systematically ground with sandpaper to remove any metallic traces of the saw-blade. The rocks were then reduced to millimetre and smaller sized pieces in a tungsten carbide hydraulic crusher by the percussion method (no grinding) and further reduced to a powder suitable for acid digestion in clean agate jars within a planetary mill.

Concentrations of the major elements and Rb, Sr, Ba, V, Ni, Cr, Zn, Ga, Y, Zr and Nb were determined by X-ray fluorescence (XRF) at the University of Massachusetts following the method of Rhodes (1996). All samples were analyzed in duplicate and the reported value is the average of the two analyses; estimates of the analytical precision and accuracy have been given by Rhodes (1996) and Rhodes & Vollinger (2004). All other trace elements were analyzed by inductively coupled plasma mass spectrometry (ICP-MS: HP 4500) at the University of Göteborg, Sweden. For each sample, approximately 12 mg of sample powder was dissolved in a solution of 1·8 ml of HF (40%) and 1·2 ml of HNO_3 (69%) for 48 h in sealed Teflon beakers on a hot plate. After evaporation, 1 ml of HNO_3 (69%) and 2 ml of H_2O (mQ) were added and the beakers were placed for 30 min in an ultrasonic bath. The resulting solution was put in a tube and an aqueous solution of 44 ml with 12 ppm Re and In was added. Each element was measured three times during a 1·5 s uptake on the ICP-MS system. Internal standard corrections were made with In or Re. After determining the blank and drift corrections, the counts/concentrations calibration line was calculated from measured counts and known concentrations of standards (89-170, AGV, K1919, BHVO, BIR, DNC and W2) and was then used to calculate element concentrations in the samples. Duplicates were made for six samples (MPC99-25, 32, 38, 45, 52 and 60). The relative differences between the two different measured concentrations for all duplicates are smaller than 5%, except for Lu (maximum 11%) and for U (less than 6% for five samples, but up to 16% for MPC99-38, which is a coarse-grained melagabbro with the lowest U concentration—0·10 ppm—of all the duplicates).

The Pb, Sr, and Nd isotopic compositions for 13 samples were measured at the Université Libre de Bruxelles on a Micromass 54 thermo-ionization multicollector mass spectrometer. For each sample, about 350 mg of powder was leached seven times with 6N HCl. The basic rocks were digested on a hot plate in closed Teflon beakers: 48 h in a solution of 10·5 ml of 6N HF and 1·5 ml of HNO_3, and an additional 24 h in 10 ml of 6N HCl. Digestion of the acidic rocks was carried out in Teflon bombs locked in metallic bombs and placed in an oven at 180°C: 96 h in HF–HNO_3 and 24 h in HCl [see Weis *et al.* (2006) for a detailed description of the procedure]. Separations of Pb, Sr and Nd were made successively on chromatographic columns (Dowex 1 × 8, Dowex W50 and HDEHP resins, respectively) following the method of Weis *et al.* (1987). For the Pb isotopic compositions, about 45 ng of Pb was loaded onto a single Re filament using the H_3PO_4–silica gel technique; for Sr isotopic compositions, about 400 ng of Sr was loaded on a single Ta filament; and for the Nd isotopic analyses, about 150 ng of Nd was loaded on a triple filament (Re and Ta). Sr isotopic ratios were normalized to $^{88}Sr/^{86}Sr = 0{\cdot}1194$ and Nd isotopic ratios were normalized to $^{146}Nd/^{144}Nd = 0{\cdot}7219$. The average $^{87}Sr/^{86}Sr$ value of the NBS 987 Sr standard was $0{\cdot}710274 \pm 13$ ($2\sigma_m$ on 18 samples) and analyses of the Merck Nd standard yielded $^{143}Nd/^{144}Nd = 0{\cdot}511958 \pm 18$ ($2\sigma_m$ on five samples). All Pb isotopic ratios were corrected for mass fractionation on the basis of analyses of the NBS 981 Pb standard for a temperature range between 1050°C and 1100°C.

For the Hf isotopic analyses, 250–300 mg of whole-rock powder for each of the 13 samples was dissolved following the procedure described by Blichert-Toft *et al.* (1997). The powders were dissolved using sub-boiled HF and HNO_3 in Savillex Teflon vials. After drying down the dissolved sample, concentrated HF was added to precipitate rare earth element (REE) fluoride salts to separate the REE from the remaining sample. High field strength elements (HFSE) were then separated from the matrix by using an anion exchange column, and Hf and Zr were isolated from the HFSE concentrate using a cation exchange column. The Hf isotopic compositions were analyzed in the static mode on a Nu Plasma multiple collector ICP-MS system (Nu 015) in the 'wet' plasma mode at the Université Libre de Bruxelles [see Weis *et al.* (2007) for a detailed description of the procedure]. Both Lu and Yb were monitored during the course of analysis for interference corrections on mass 176; the ^{172}Yb beam was negligible. The measured Hf isotopic ratios were corrected for isobaric interference with

Lu at mass 176 by monitoring the isotope ^{175}Lu; the ^{176}Lu interference was subtracted using a value of 37·69969 for $^{176}Lu/^{175}Lu$ (Rosman & Taylor, 1998). During the analyses, replicate measurements of the Hf JMC 475 in-house standard gave 0·282164 ± 15 ($2\sigma_m$ on 13 measurements) and 0·282173 ± 13 ($2\sigma_m$ on 13 measurements) for the two analytical sessions, which is within the range of previously published values for this standard (e.g. Blichert-Toft *et al.*, 1997; Chauvel & Blichert-Toft, 2001; Goolaerts *et al.*, 2004). For consistency, all values were normalized to $^{176}Hf/^{177}Hf = 0·282160$.

GEOCHEMISTRY OF THE VAL GABBRO PLUTONIC SUITE

The major and trace element chemistry of whole-rock samples from the Val gabbro plutonic suite is reported in Table 2 and the isotopic chemistry is presented in Table 3 (Sr, Nd, Hf) and Table 4 (Pb).

Major element variations

Intrusive rocks of the Val gabbro plutonic suite, including new analyses from this study and from the earlier study of Giret & Beaux (1984) (data normalized to 100 wt %), span a wide range of SiO_2 contents from 43 wt % for the peridotites to 67 wt % for the felsic rocks, with a corresponding range in MgO contents from 28 to 0·42 wt %, respectively (Fig. 7). There are three main compositional groups with respect to major elements: (1) microgabbros and subophitic microgabbros; (2) felsic rocks; (3) peridotites; the equigranular gabbros generally extend from the field of the microgabbros towards the peridotites (Fig. 7).

The compositions of the microgabbros and subophitic microgabbros overlap with those of the host mildly alkalic basalts and many of the basaltic lavas analyzed from the Southeast Province (Fig. 7) (Weis *et al.*, 1993; Frey *et al.*, 2000). With the exception of sample MPC99-52, which contains abundant olivine, the microgabbros show only limited geochemical variation (e.g. 5–6 wt % MgO, 48–49 wt % SiO_2). There is a distinct compositional gap in silica between the microgabbros and the felsic rocks, and the felsic rocks overlap in composition with trachytic lavas from the Southeast Province (Weis *et al.*, 1993; Frey *et al.*, 2000) (Fig. 7). In addition to being characterized by relatively low SiO_2 and high MgO contents, the peridotites have low total alkalis and low Al_2O_3, reflecting a dilution effect of all elements not compatible in olivine and/or clinopyroxene. In Fig. 7, the compositions of olivine and clinopyroxene cores from the peridotites are plotted for comparison with the whole-rock compositions. MgO contents in the peridotites vary from 13 to 28 wt % and the olivine-rich rocks (wehrlites) extend along a mineral control line between the region represented by the microgabbros and end-member olivine compositions of $\sim Fo_{80–85}$. The clinopyroxene-rich rocks (olivine clinopyroxenites) plot systematically towards the field for the measured clinopyroxene compositions (Fig. 7: see $Na_2O + K_2O$ and CaO vs SiO_2). The major element compositions of the equigranular gabbros are variable (Fig. 7), reflecting the variable modal proportion of plagioclase to clinopyroxene (± olivine and Fe–Ti oxides) in these rocks: (1) clinopyroxene-rich samples (MPC99-30, 31, 44, 58) trend towards the field for clinopyroxene compositions defined by the peridotites; (2) plagioclase-rich rocks (e.g. MPC99-45) have higher alumina contents (up to 21·2 wt %) characteristic of intermediate to calcic plagioclase; (3) sample MPC99-46, which has abundant olivine, plots towards the field for the peridotites and has elevated MgO (13·1 wt %) relative to all other equigranular gabbros; (4) sample MPC99-59, which has abundant euhedral Fe–Ti oxides, has high TiO_2 contents (5·1 wt %). The correlation between modal abundances and whole-rock geochemistry for the equigranular gabbros suggests that they represent cumulates of primarily plagioclase and clinopyroxene, with the notable exceptions of samples MPC99-46 and 59, which also contain cumulus olivine and Fe–Ti oxides, respectively.

Trace element variations

There is a strong positive correlation between Nb, which shows a large variation in the sample suite from 2 to 104 ppm and is relatively immobile during low-temperature alteration, and incompatible elements that are sensitive to secondary alteration (e.g. K, Rb, and Ba) (Fig. 8). This demonstrates that most samples from the Val gabbro plutonic suite have remained closed since their time of crystallization without significant loss or gain of these mobile elements. All of the basic rocks and basalts from the Southeast Province are characterized by similar incompatible element ratios (e.g. K/Nb, Rb/Nb, Zr/Nb, Th/Nb), which is consistent with their formation from common parental magmas. When incompatible elements are compared, the peridotites and equigranular gabbros plot close to the origin of the graphs, as a result of accumulation of olivine and clinopyroxene and the dilution effect on incompatible elements (Fig. 8). The equigranular gabbros have slightly higher K (and Ba) concentrations for given Nb values than the peridotites and microgabbros (Fig. 8), which is probably due to accumulation of plagioclase in these rocks. Elevated Sr concentrations at low Nb contents for the majority of the equigranular gabbros, and especially the extremely high Sr concentration of sample MPC99-45 (915 ppm) (Fig. 8), are consistent with significant plagioclase accumulation. The effect of clinopyroxene accumulation in the peridotites and equigranular gabbros is demonstrated by their elevated Sc concentration, which is compatible in clinopyroxene, with decreasing Nb (Fig. 8) (note that samples with low Sc concentrations, <25 ppm, are relatively olivine-rich and clinopyroxene-poor). In contrast, the effect of clinopyroxene fractionation in the microgabbros and especially in basalts from the Southeast

Table 2: Major element (wt % oxides) and trace element (ppm) abundances in samples from the Val gabbro plutonic suite and surrounding basalts

MPC99:	32	34	38	39	36	40	41	30	31	44	45	46
Type:	WEHR	WEHR	WEHR	WEHR	OLCPX	OLCPX	OLCPX	EG	EG	EG	EG	EG
SiO_2	43·77	44·93	43·34	44·15	46·86	45·40	47·31	48·52	49·12	48·74	49·48	45·54
TiO_2	1·33	0·84	0·71	0·93	1·50	0·73	1·09	1·56	1·71	1·38	2·73	1·53
Al_2O_3	6·17	6·55	5·62	5·25	7·86	8·14	11·46	16·22	15·32	19·01	21·21	13·66
Fe_2O_3	14·06	13·42	14·54	15·31	12·81	12·40	10·20	8·72	9·23	7·11	7·91	12·43
MnO	0·19	0·19	0·20	0·21	0·19	0·18	0·16	0·14	0·14	0·11	0·10	0·17
MgO	26·79	23·27	27·76	24·41	16·71	19·23	13·35	8·30	8·28	6·40	3·08	13·06
CaO	6·15	9·59	6·72	8·88	12·32	12·87	15·19	14·11	12·90	14·62	10·55	11·66
Na_2O	0·82	0·74	0·55	0·54	0·71	0·69	0·70	1·70	1·96	2·08	3·05	1·10
K_2O	0·42	0·37	0·23	0·14	0·48	0·12	0·15	0·60	0·98	0·54	1·32	0·59
P_2O_5	0·17	0·07	0·08	0·08	0·13	0·03	0·08	0·14	0·18	0·15	0·31	0·14
Total	99·87	99·96	99·74	99·88	99·54	99·79	99·68	100·01	99·82	100·13	99·72	99·89
mg-no.	0·79	0·77	0·79	0·76	0·72	0·75	0·72	0·65	0·64	0·64	0·44	0·68
AI	−0·53	−1·10	−0·82	−1·23	−1·72	−1·55	−2·23	−1·22	−0·80	−0·99	0·50	−0·73
Rb	11·8	9·4	7·2	3·9	13·1	2·1	2·6	11·3	21·5	10·2	26·4	12·7
Sr	194	177	160	110	226	235	369	435	464	550	915	510
Ba	126	77	78	31	132	56	82	154	191	169	417	171
Sc	20·6	33·9	21·8	31·6	44·5	44·7	51·5	38·6	42·3	37·6	18·3	33·3
V	128	163	100	156	246	149	187	183	189	165	181	193
Cr	1363	1206	1422	1287	1197	1467	946	422	256	415	17	332
Co	117	109	122	113	85	91	62	39	41	31	26	76
Ni	897	624	917	697	342	533	271	126	120	62	32	214
Zn	106	95	110	111	94	83	72	71	74	58	58	85
Ga	10	8	8	8	12	9	14	18	19	19	26	16
Y	10·6	7·6	6·8	8·7	12·7	6·7	10·7	12·6	14·3	14·5	15·4	11·3
Zr	79	45	45	41	78	26	40	79	82	97	181	92
Nb	12·6	5·3	5·8	6·8	9·7	1·8	3·2	10·5	11·0	14·8	27·2	13·3
Hf	1·8	1·2	1·1	1·0	2·4	0·9	1·6	1·7	1·7	2·1	*3·8*	2·3
Th	1·28	0·73	0·62	0·40	1·36	0·21	0·31	1·11	1·17	1·92	3·00	1·79
U	0·25	0·15	0·11	0·08	0·29	0·04	0·07	0·20	0·15	0·38	0·42	0·33
Pb	1·04	0·47	0·57	1·02	0·95	0·57	0·96	2·65	1·46	1·99	3·03	1·33
La	12·0	5·89	6·21	5·79	10·5	3·73	5·88	12·3	12·7	14·7	26·4	12·9
Ce	25·0	12·8	13·3	13·0	23·1	8·50	13·8	25·8	27·4	31·0	53·3	26·9
Pr	3·17	1·74	1·71	1·77	3·05	1·23	2·03	3·42	3·63	3·90	6·42	3·42
Nd	13·0	7·49	7·26	7·83	13·2	5·80	9·58	14·7	15·6	15·9	24·9	14·0
Sm	2·96	1·90	1·72	1·92	3·20	1·50	2·51	3·45	3·74	3·64	5·35	3·27
Eu	0·97	0·65	0·60	0·66	1·07	0·60	1·00	1·22	1·32	1·26	1·85	1·14
Gd	2·94	2·08	1·79	2·10	3·38	1·73	2·84	3·50	3·78	3·60	4·63	3·10
Tb	0·44	0·32	0·29	0·32	0·53	0·28	0·45	0·54	0·59	0·56	0·70	0·47
Dy	2·37	1·76	1·51	1·82	2·96	1·55	2·46	2·90	3·19	3·12	3·53	2·53
Ho	0·43	0·31	0·27	0·32	0·53	0·27	0·45	0·50	0·56	0·58	0·61	0·45
Er	1·11	0·80	0·70	0·85	1·36	0·70	1·14	1·28	1·43	1·54	1·54	1·13
Yb	0·90	0·65	0·57	0·70	1·07	0·58	0·89	1·01	1·06	1·29	1·20	0·94
Lu	0·15	0·11	0·09	0·11	0·17	0·09	0·14	0·15	0·16	0·20	0·20	0·15
Eu/Eu*	1·02	1·02	1·05	1·02	1·00	1·15	1·14	1·08	1·07	1·07	1·15	1·10

(continued)

Table 2: Continued

MPC99:	58	59	60	23	28	51	52	54	24	25	26	47
Type:	EG	EG	EG	MG	MG	MG	MG	MG	SMG	SMG	SMG	FR
SiO_2	49·07	45·44	48·61	48·47	48·83	47·97	46·80	48·69	49·10	48·86	49·04	59·45
TiO_2	1·72	5·05	2·86	3·20	2·90	3·29	2·47	2·50	3·23	3·36	3·32	0·97
Al_2O_3	17·77	14·07	16·93	14·31	14·49	14·82	12·03	16·65	14·24	14·13	14·25	18·15
Fe_2O_3	8·63	15·03	11·08	13·27	12·29	13·51	12·24	11·01	13·23	13·38	13·35	6·69
MnO	0·12	0·21	0·16	0·18	0·17	0·19	0·18	0·16	0·18	0·18	0·19	0·09
MgO	6·58	5·26	5·07	5·64	6·02	5·51	11·60	5·91	5·00	4·94	4·89	1·14
CaO	13·25	10·67	11·15	10·37	10·85	9·48	11·07	10·94	9·29	9·35	9·36	3·15
Na_2O	2·11	2·73	2·77	2·85	2·76	3·17	2·15	2·68	3·31	3·12	3·16	5·17
K_2O	0·74	0·91	1·15	1·43	1·31	1·75	1·04	1·09	1·88	1·79	1·86	4·93
P_2O_5	0·16	0·33	0·30	0·46	0·42	0·45	0·27	0·30	0·54	0·54	0·56	0·24
Total	100·15	99·69	100·08	100·17	100·03	100·14	99·84	99·92	100·00	99·65	99·96	99·98
mg-no.	0·60	0·41	0·48	0·46	0·49	0·45	0·65	0·52	0·43	0·42	0·42	0·25
Al	−0·88	1·26	0·37	0·77	0·43	1·61	0·30	0·18	1·45	1·26	1·30	2·54
Rb	15·5	18·3	23·0	29·6	26·3	35·8	28·2	25·0	40·7	39·2	39·0	79·7
Sr	548	531	586	523	525	466	377	485	531	527	523	344
Ba	239	279	306	362	337	397	276	309	439	432	436	688
Sc	31·8	31·6	27·6	26·2	27·4	26·0	33·9	27·2	25·1	24·1	25·0	5·8
V	179	403	250	285	242	307	257	236	239	246	243	21
Cr	168	0	32	64	140	52	482	81	12	14	15	2
Co	36	50	42	44	43	44	62	41	47	43	42	9
Ni	92	9	47	56	67	58	298	50	43	41	40	5
Zn	65	99	86	111	98	130	103	78	123	124	132	74
Ga	20	24	23	23	22	24	18	23	25	25	25	27
Y	13·6	23·4	19·5	23·8	22·5	28·5	19·8	22·1	27·2	27·1	27·4	31·0
Zr	94	154	153	208	194	230	152	176	247	241	245	697
Nb	12·8	26·7	24·4	33·9	31·8	35·3	29·0	30·0	40·1	39·7	39·7	52·6
Hf	2·2	3·2	*3·4*	4·4	5·0	*4·9*	*4·0*	*4·2*	5·2	5·1	5·6	*7·3*
Th	1·62	2·26	2·55	3·45	3·36	3·55	2·59	3·15	4·34	4·23	4·50	5·51
U	0·32	0·31	0·37	0·68	0·65	0·61	0·45	0·47	0·86	0·75	0·80	0·92
Pb	2·26	1·97	2·65	2·60	2·28	2·78	1·81	2·58	3·41	2·56	3·01	7·13
La	14·3	22·9	22·2	31·2	29·4	33·2	22·8	26·8	41·5	37·2	39·5	52·7
Ce	30·2	48·7	47·2	66·0	62·0	67·3	47·9	55·9	88·2	78·8	83·1	105
Pr	3·81	6·24	5·84	8·12	7·61	8·46	5·91	6·93	10·3	9·68	10·1	11·9
Nd	15·7	26·3	23·7	32·2	30·3	33·7	24·0	27·5	39·9	38·3	39·7	43·7
Sm	3·61	6·07	5·23	7·20	6·66	7·51	5·34	6·04	8·80	8·39	8·67	8·79
Eu	1·31	2·11	1·81	2·30	2·20	2·37	1·71	1·95	2·75	2·67	2·72	2·78
Gd	3·68	6·14	5·20	6·74	6·38	7·12	5·19	5·81	8·07	7·97	8·19	7·21
Tb	0·56	0·93	0·78	1·00	0·94	1·06	0·79	0·86	1·21	1·16	1·20	1·05
Dy	3·09	5·04	4·14	5·26	5·01	5·71	4·30	4·74	6·31	6·00	6·31	5·45
Ho	0·56	0·89	0·75	0·91	0·89	1·02	0·79	0·87	1·08	1·04	1·11	0·96
Er	1·41	2·29	1·87	2·34	2·26	2·72	2·01	2·24	2·75	2·61	2·82	2·49
Yb	1·08	1·74	1·43	1·78	1·70	2·13	1·65	1·78	2·05	1·93	2·09	1·98
Lu	0·17	0·27	0·20	0·28	0·29	0·29	0·24	0·25	0·31	0·30	0·33	0·27
Eu/Eu*	1·11	1·07	1·08	1·01	1·04	1·00	1·01	1·01	1·00	1·02	1·00	1·07

(continued)

Table 2: Continued

MPC99:	49	50	53a/A	53b/A	53c/A	56	57	42	53a/B	53c/B	61	62
Type:	FR	FR	FR	FR	FR	FR	FR	SEB	SEB	SEB	SEB	SEB
SiO_2	64·30	63·58	63·80	64·03	63·39	61·86	67·18	49·38	48·10	49·10	48·38	48·30
TiO_2	0·50	0·94	0·90	0·92	1·03	1·32	0·98	3·35	3·11	3·26	2·87	2·87
Al_2O_3	17·87	17·43	16·80	16·61	17·42	16·05	16·25	16·19	17·02	16·34	16·60	16·57
Fe_2O_3	3·82	3·59	5·81	5·80	4·39	6·65	2·34	13·05	13·38	12·00	11·81	11·82
MnO	0·07	0·04	0·05	0·04	0·04	0·12	0·03	0·21	0·21	0·18	0·14	0·16
MgO	0·42	1·46	1·24	1·24	1·24	1·26	0·68	4·87	4·81	4·29	5·88	6·24
CaO	1·58	1·24	2·03	1·77	1·89	3·20	1·06	8·61	8·82	9·85	9·95	9·50
Na_2O	5·62	4·95	4·55	4·53	4·11	4·29	3·23	2·59	3·29	2·90	2·86	3·05
K_2O	5·71	6·41	4·74	4·90	6·37	5·06	7·88	1·18	1·23	1·42	1·19	1·15
P_2O_5	0·10	0·21	0·25	0·26	0·22	0·34	0·21	0·46	0·40	0·44	0·35	0·33
Total	99·98	99·86	100·16	100·09	100·11	100·14	99·84	99·88	100·36	99·77	100·04	99·99
mg-no.	0·18	0·45	0·30	0·30	0·36	0·27	0·37	0·42	0·42	0·41	0·50	0·51
AI	1·97	2·27	0·11	0·17	1·45	0·90	0·69	−0·08	1·16	0·59	0·58	0·76
Rb	112	122	101	95·0	138	125	169	25·7	26·8	26·4	19·8	20·0
Sr	207	201	320	333	304	268	302	442	441	505	459	442
Ba	666	730	890	910	908	780	688	245	336	355	261	249
Sc	3·1	5·3	5·4	6·7	4·6	9·0	4·7	25·7	24·5	26·0	25·3	26·7
V	3	49	22	28	52	47	26	312	271	298	251	256
Cr	2	25	5	2	11	5	19	20	76	235	150	94
Co	3	7	8	9	7	12	6	37	37	30	39	41
Ni	1	18	3	4	13	8	11	34	43	63	64	64
Zn	51	31	43	41	44	80	21	86	121	120	102	104
Ga	27	27	28	26	27	27	27	24	25	24	23	23
Y	35·6	41·0	47·9	43·4	39·4	46·9	32·5	27·7	28·9	29·9	22·4	22·5
Zr	518	777	597	578	689	712	681	250	212	223	179	171
Nb	78·2	101·3	77·2	76·4	99·7	60·1	104·2	38·0	34·2	36·4	27·8	27·4
Hf	*10·9*	*14·1*	*10·7*	*10·6*	*13·8*	*8·3*	*14·5*	*5·3*	*4·8*	*5·1*	4·4	4·4
Th	12·3	13·7	11·4	13·4	12·7	13·1	17·7	3·53	3·34	3·68	3·07	3·09
U	1·99	2·25	1·62	1·72	2·29	1·17	1·64	0·77	0·62	0·49	0·63	0·47
Pb	7·87	5·49	5·62	5·60	8·91	7·56	4·03	2·71	4·17	4·04	2·69	1·83
La	57·4	71·0	56·1	64·8	59·0	64·4	71·3	32·0	30·9	34·2	24·4	23·8
Ce	118	141	113	132	118	127	142	67·6	61·6	63·7	51·9	50·7
Pr	13·2	15·1	12·5	14·7	12·6	14·7	15·4	8·31	8·05	8·58	6·43	6·31
Nd	47·6	51·7	44·8	52·7	43·5	53·1	52·3	33·5	32·6	35·2	26·5	26·0
Sm	9·53	9·92	9·14	10·7	8·54	11·3	10·4	7·25	7·35	7·71	5·82	5·78
Eu	2·62	2·59	2·43	2·84	2·19	3·10	2·43	2·36	2·30	2·42	1·91	1·90
Gd	8·22	8·42	8·36	9·44	7·52	10·4	8·43	7·24	7·18	7·44	5·94	5·86
Tb	1·21	1·21	1·22	1·38	1·09	1·58	1·22	1·07	1·10	1·12	0·88	0·88
Dy	6·72	6·87	6·95	7·97	6·32	9·30	6·57	5·87	6·05	6·16	4·90	4·92
Ho	1·18	1·20	1·32	1·47	1·18	1·73	1·16	1·03	1·10	1·10	0·90	0·90
Er	3·06	3·12	3·47	3·84	3·14	4·57	2·92	2·55	2·86	2·85	2·33	2·34
Yb	2·45	2·64	2·92	3·16	2·56	3·96	2·42	1·98	2·26	2·14	1·92	1·87
Lu	0·32	0·35	0·37	0·41	0·33	0·52	0·33	0·28	0·31	0·30	0·31	0·31
Eu/Eu^*	0·91	0·88	0·86	0·87	0·85	0·88	0·81	1·00	0·98	0·98	1·01	1·01

WEHR, wehrlite; OLCPX, olivine clinopyroxenite; EG, equigranular gabbro; MG, microgabbro; SMG, subophitic microgabbro; FR, felsic rocks; SEB, Southeast Province basalts. XRF was used to measured the major elements and the trace elements Rb, Sr, Ba, V, Ni, Cr, Zn, Ga, Y, Zr and Nb; element abundances were measured by XRF after heating samples at 1000°C to oxidize the iron to Fe^{3+} and to remove volatiles. Other trace elements were determined by ICP-MS. Hf values in italics were estimated from average $Nb/Hf = 7{\cdot}2$ ($1\sigma = 0{\cdot}6$) defined by samples from the Val gabbro plutonic suite and volcanic rocks from the Southeast Province (Weis *et al.*, 1993; Frey *et al.*, 2000). mg-no. is calculated as the cationic ratio $Mg^{2+}/(Mg^{2+} + Fe_{tot}{}^{2+})$. AI is the Alkalinity Index and is calculated as $Na_2O + K_2O - (0{\cdot}37SiO_2 + 14{\cdot}43)$. $E/Eu^* = Eu_{CN}/[(Sm_{CN})(Gd_{CN})]^{1/2}$, where CN is the chondrite-normalized value.

Table 3: Sr, Nd and Hf isotopic ratios and parent/daughter abundance ratios (calculated from data in Table 2) of samples from the Val gabbro plutonic suite

Sample	Rock type	$^{87}Rb/^{86}Sr$	$^{87}Sr/^{86}Sr(m)$	2σm	$^{87}Sr/^{86}Sr(i)$	$^{147}Sm/^{144}Nd$	$^{143}Nd/^{144}Nd(m)$	2σm	$^{143}Nd/^{144}Nd(i)$	εNd(i)	$^{176}Lu/^{177}Hf$	$^{176H}f/^{177}Hf(m)$	2σm	$^{176}Hf/^{177}Hf(i)$	εHf(i)
MPC99-34	Wehrlite	0·1537	0·705056	9	0·70500	0·1535	0·512632	8	0·51261	0·02	0·0131	0·282831	11	0·282825	2·43
MPC99-38	Wehrlite	0·1302	0·705140	7	0·70510	0·1439	0·512626	8	0·51260	−0·07	0·0115	0·282799	9	0·282794	1·31
MPC99-36	Olivine clinopyroxenite	0·1677	0·705060	7	0·70500	0·1463	0·512635	10	0·51261	0·10	0·0105	0·282827	12	0·282822	2·31
MPC99-40	Olivine clinopyroxenite	0·0259	0·705217	7	0·70521	0·1567	0·512616	9	0·51259	−0·31	0·0138	0·282798	14	0·282792	1·24
MPC99-45	Equigranular gabbro	0·0835	0·705273	7	0·70524	0·1305	0·512575	11	0·51255	−1·03	0·0092	0·282762	13	0·282758	0·05
MPC99-46	Equigranular gabbro	0·0721	0·705362	7	0·70534	0·1413	0·512580	8	0·51256	−0·96	0·0095	0·282747	9	0·282743	−0·48
MPC99-60	Equigranular gabbro	0·1136	0·705284	6	0·70525	0·1341	0·512567	7	0·51255	−1·19	0·0058	0·282784	9	0·282781	0·86
MPC99-51	Microgabbro	0·2223	0·705269	6	0·70519	0·1347	0·512581	7	0·51256	−0·92	0·0138	0·282799	15	0·282793	1·28
MPC99-24	Subophitic microgabbro	0·2218	0·705232	7	0·70516	0·1332	0·512588	6	0·51257	−0·78	0·0085	0·282789	6	0·282785	1·00
MPC99-25	Subophitic microgabbro	0·2153	0·705248	6	0·70517	0·1322	0·512586	8	0·51257	−0·82	0·0086	0·282794	6	0·282790	1·18
MPC99-47	Felsic rock	0·6705	0·705576	7	0·70535	0·1217	0·512590	10	0·51257	−0·71	0·0085	0·282770	18	0·282766	0·34
MPC99-53a/A	Felsic rock	0·9161	0·705491	8	0·70518	0·1234	0·512621	8	0·51260	−0·11	0·0082	0·282837	14	0·282833	2·69
MPC99-57	Felsic rock	1·6157	0·705764	7	0·70521	0·1199	0·512616	10	0·51260	−0·19	0·0079	0·282796	13	0·282793	1·28
MPC99-34 (NL)	Wehrlite		0·705125	8	0·70513		0·512620	8	0·51262	0·25					
MPC99-51 (REP)	Microgabbro											0·282792	17		
MPC99-24 (RERUN)	Subophitic microgabbro											0·282781	9		
MPC99-53a/A (DUP)	Felsic rock	0·6520	0·705428	7	0·70521	0·1228	0·512622	8	0·51260	−0·09					
MPC99-53a/A (NL)	Felsic rock		0·705498	6	0·70550		0·512596	10	0·51260	−0·22					

All samples are leached, except for those indicated by NL (non-leached). RERUN indicates a re-run during the same analytical session; REP indicates a replicate analysis during a different analytical session; DUP indicates a complete analytical duplicate. (m) indicates measured ratios and (i) indicates age-corrected ratios to 24 Ma; for age corrections, Rb and Sr concentrations are by XRF, and Sm, Nd, Lu, and Hf concentrations are by ICP-MS.

Province is shown by progressively decreasing Sc concentrations with increasing Nb.

The felsic rocks have the highest incompatible element concentrations of the sample suite (e.g. up to 104 ppm Nb, 777 ppm Zr, and 18 ppm Th; Table 2). Incompatible element ratios in the felsic rocks vary considerably with respect to the other rock types of the Val gabbro plutonic suite. For example, Zr/Nb is similar, K/Nb and Rb/Nb higher, and La/Nb lower in the felsic rocks compared with the peridotites, gabbros and basalts (Fig. 8). These variations mostly reflect changes in the relative compatibility of some trace elements as a result of the crystallizing assemblage (plag ± ksp ± ilm ± amph ± fa ± cpx ± zirc ± apa), which is significantly different from that of the microgabbros and basalts (plag + cpx ± ol) discussed above. In particular, Nb is compatible in ilmenite in differentiated basaltic magmas (Jang & Naslund, 2003) and differentiated flood basalts on the Kerguelen Archipelago are ilmenite ± titanomagnetite-saturated at MgO <4 wt % (see Scoates *et al.*, 2006, fig. 4). The two felsic rock samples with the lowest SiO_2 contents (MPC99-47 and 56) have anomalously low Nb concentrations relative to the other felsic rocks and the trachytes from the Southeast Province (Fig. 8). Sample MPC99-47 is plagioclase-rich, contains no quartz, and has a small positive Eu anomaly ($Eu/Eu^* = 1·07$ compared with the typical range of 0·81–0·91 for the other felsic rocks; Table 2), which indicates that feldspar accumulation plays a role in the anomalous chemistry. Sample MPC99-56 has strongly altered feldspar, which may explain the high Rb concentration (125 ppm), and also contains numerous, small (1–3 mm) fine-grained plagioclase- and oxide-rich inclusions, indicating that the sample does not represent a melt composition.

Primitive mantle-normalized incompatible element patterns for all of the basic rocks in the Val gabbro plutonic suite and the host basalts are shown in Fig. 9. The cumulates have the lowest trace element abundances and flattest patterns, whereas the zircon-bearing subophitic microgabbros have the highest abundances and steepest patterns. Two plagioclase-bearing wehrlites (MPC99-34 and 38), two olivine clinopyroxenites (MPC99-40 and 41), and all of the equigranular gabbros have strong positive Sr anomalies (Fig. 9) and small positive Eu anomalies in chondrite-normalized plots ($Eu/Eu^* = 1·02$ and 1·05 in the wehrlites,

Table 4: Pb isotopic ratios and parent/daughter abundance ratios (calculated from data in Table 2) of samples from the Val gabbro plutonic suite

Sample	Rock type	$^{206}Pb/^{204}Pb(m)$	$^{207}Pb/^{204}Pb(m)$	$^{208}Pb/^{204}Pb(m)$	$^{238}U/^{204}Pb$	$^{235}U/^{204}Pb$	$^{232}Th/^{204}Pb$	$^{206}Pb/^{204}Pb(i)$	$^{207}Pb/^{204}Pb(i)$	$^{208}Pb/^{204}Pb(i)$
MPC99-34	Wehrlite	18·512	15·555	39·09	19·9	0·1444	102·8	18·44	15·56	39·08
MPC99-38	Wehrlite	18·488	15·536	39·05	12·8	0·0932	72·4	18·44	15·54	39·04
MPC99-36	Olivine clinopyroxenite	18·464	15·541	39·01	19·7	0·1427	94·6	18·39	15·54	39·00
MPC99-40	Olivine clinopyroxenite	18·435	15·531	38·98	4·4	0·0322	24·7	18·42	15·53	38·97
MPC99-45	Equigranular gabbro	18·250	15·516	38·78	8·8	0·0636	65·4	18·22	15·52	38·76
MPC99-46	Equigranular gabbro	18·348	15·537	38·93	15·8	0·1147	88·6	18·29	15·54	38·92
MPC99-60	Equigranular gabbro	18·412	15·543	38·97	9·0	0·0652	63·6	18·38	15·54	38·95
MPC99-51	Microgabbro	18·449	15·531	38·99	14·1	0·1024	84·5	18·40	15·53	38·96
MPC99-24	Subophitic microgabbro	18·331	15·504	38·83	16·0	0·1163	83·7	18·27	15·50	38·79
MPC99-25	Subophitic microgabbro	18·367	15·539	38·91	18·6	0·1352	108·8	18·30	15·54	38·87
MPC99-47	Felsic rock	18·310	15·537	38·89	8·2	0·0594	50·9	18·28	15·54	38·86
MPC99-53a/A	Felsic rock	18·446	15·556	39·07	18·4	0·1335	133·7	18·38	15·56	39·00
MPC99-57	Felsic rock	18·508	15·558	39·09	26·0	0·1885	290·9	18·41	15·56	38·94
MPC99-34 (NL)	Wehrlite	18·104	15·603	38·02						
MPC99-51 (REP)	Microgabbro	18·475	15·551	39·04						
MPC99-24 (RERUN)	Subophitic microgabbro	18·368	15·537	38·93						
MPC99-24 (REP)	Subophitic microgabbro	18·389	15·563	39·00						
MPC99-25 (RERUN)	Subophitic microgabbro	18·378	15·545	38·94						
MPC99-25 (REP)	Subophitic microgabbro	18·385	15·555	38·97						
MPC99-47 (RERUN)	Felsic rock	18·307	15·534	38·88						
MPC99-47 (REP)	Felsic rock	18·307	15·535	38·88						
MPC99-53a/A (DUP)	Felsic rock	18·492	15·562	39·08	18·8	0·1365	168·3	18·42	15·56	39·00

All samples are leached, except for those indicated by NL (non-leached). RERUN indicates a re-run during the same analytical session; REP indicates a replicate analysis during a different analytical session; DUP indicates a complete analytical duplicate. (m) indicates measured ratios and (i) indicates age-corrected ratios to 24 Ma; for age corrections, Pb, U and Th concentrations are by ICP-MS. 2σ errors are 0·1% for $^{206}Pb/^{204}Pb$ and $^{207}Pb/^{204}Pb$, and 0·15% for $^{208}Pb/^{204}Pb$.

1·14 and 1·15 in the olivine clinopyroxenites, and 1·07–1·15 in the equigranular gabbros; Table 2), which is consistent with the presence of cumulus plagioclase in these samples. The relatively small positive Eu anomalies compared with the Sr anomalies in these rocks suggest that the positive Eu anomaly provided by cumulus plagioclase is offset by the negative anomaly typically associated with cumulus clinopyroxene (e.g. McKay, 1989). The small positive Ti anomaly in sample MPC99-59 correlates with the presence of accumulated Fe–Ti oxides (ilmenite). The microgabbros have primitive mantle-normalized patterns that are very similar to those of the mildly alkalic basalts from the Southeast Province (Weis *et al.*, 1993; Frey *et al.*, 2000) and the host basalts (Fig. 9), confirming that the microgabbros represent melt to near-melt compositions.

Sr, Nd, Pb, and Hf isotopic compositions

Age-corrected isotopic ratios for acid-leached samples from the Val gabbro plutonic suite are plotted in Fig. 10 (age corrections are for *in situ* decay over 24 Myr, based on measured parent–daughter concentrations from non-leached powders reported in Table 2). Analyses of non-leached (NL) aliquots are reported for several samples in Table 3 (MPC99-34 and 53 a/A) and Table 4 (MPC99-34). The efficient removal of secondary alteration phases by leaching is demonstrated by the lower $^{87}Sr/^{86}Sr$ and higher $^{206}Pb/^{204}Pb$ and $^{208}Pb/^{204}Pb$ of the leached (measured) aliquots. Samples from the Val gabbro plutonic suite show a relatively restricted range of isotopic compositions, which suggests that all intrusive rocks are genetically related to parent magmas of broadly similar isotopic composition. Initial $^{87}Sr/^{86}Sr$ is negatively correlated with initial $^{143}Nd/^{144}Nd$, and these ratios range from 0·70500 to 0·70535 and from 0·51254 to 0·51262, respectively. The initial ε_{Nd} and initial ε_{Hf} values are positively correlated, spanning a small range from −1·19 to +0·25 and −0·02 to 3·16, respectively. The Pb isotopic compositions are also positively correlated, with initial

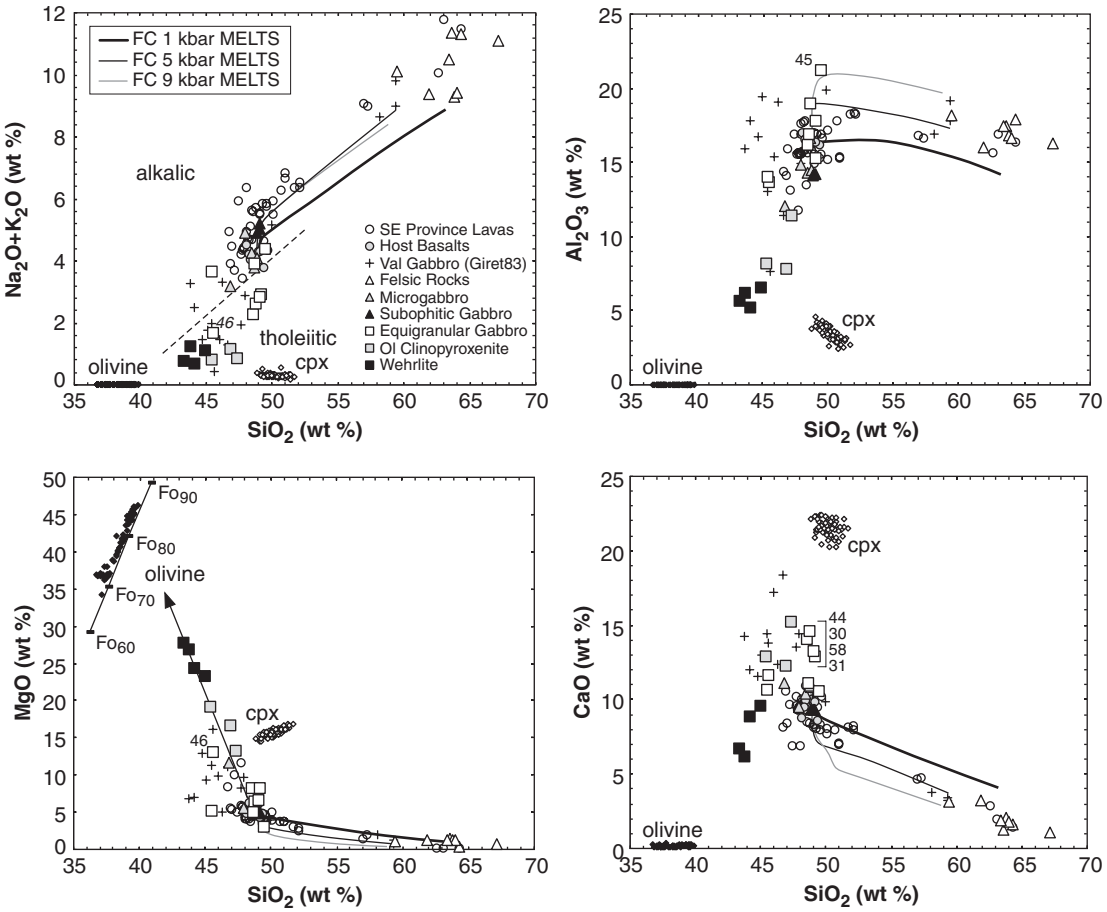

Fig. 7. Total alkalis ($Na_2O + K_2O$) and major element oxides vs SiO_2 variation diagrams showing samples from this study, previous analyses from Giret (1983) (+), volcanic rocks from Southeast Province (Weis *et al.*, 1993; Frey *et al.*, 2000), and olivine and clinopyroxene core compositions from the coarse-grained peridotites from the Val gabbro plutonic suite. The tholeiitic–alkalic limit from MacDonald & Katsura (1964) is shown as a dashed line in the total alkalis vs SiO_2 plot. A line with the range of olivine forsterite contents from Fo_{60} to Fo_{90} is indicated for reference in the MgO vs SiO_2 plot. Samples referred to in the text are labeled. Fractional crystallization trends calculated with MELTS (Ghiorso & Sack, 1995) are shown for 1, 5, and 9 kbar from a starting composition equivalent to MPC99-54, an aphyric microgabbro ($fO_2 = FMQ - 1$; starting water content 0·75 wt % H_2O; the high-SiO_2 end of each calculated trend represents 26–27% remaining liquid) (see Discussion for interpretation).

$^{206}Pb/^{204}Pb = 18{\cdot}22–18{\cdot}44$, $^{207}Pb/^{204}Pb = 15{\cdot}50–15{\cdot}56$, and $^{208}Pb/^{204}Pb = 38{\cdot}76–39{\cdot}08$ (note the relatively large size of the 2σ error in $^{207}Pb/^{206}Pb$ compared with the total range observed for the Val gabbro plutonic suite). Within the isotopic dataset, the peridotites show a small but systematic difference from the other samples (Fig. 10), with relatively low $^{87}Sr/^{86}Sr$ and high $^{143}Nd/^{144}Nd$, $^{176}Hf/^{177}Hf$ and Pb isotopic ratios compared with the other rocks. In contrast, the equigranular gabbros are characterized by relatively high initial $^{87}Sr/^{86}Sr$ and low $^{143}Nd/^{144}Nd$ and $^{176}Hf/^{177}Hf$ (Fig. 10). The isotopic compositions of the microgabbros generally plot closer to the equigranular gabbros and those of the felsic rocks span the range from the peridotites to equigranular gabbros (Fig. 10). These small isotopic differences between the rock types in the Val gabbro plutonic suite are consistent with emplacement of distinct magma batches within an open-system sub-volcanic intrusion.

DISCUSSION

Prior to this study, it was considered that the Val gabbro plutonic suite formed from a tholeiitic parent magma on the Kerguelen Archipelago at 39 Ma (Giret & Lameyre, 1984; Giret & Beaux, 1984). Re-investigation of the age, petrology and geochemistry of a new sample suite from the intrusion reveals the following: (1) the intrusion was emplaced at 24 Ma at relatively shallow levels (e.g. extensive brecciation of overlying host basalts, limited contact metamorphic effects) into the 25 Ma mildly alkalic basalts that represent the majority of the Southeast Province; (2) the microgabbros and most of the fine-grained felsic rocks in the intrusion represent melt or near-melt compositions and they overlap in major and trace element geochemistry with alkalic basalts and trachytes, respectively, from the Southeast Province; (3) the peridotites and equigranular gabbros are cumulate rocks formed by the accumulation

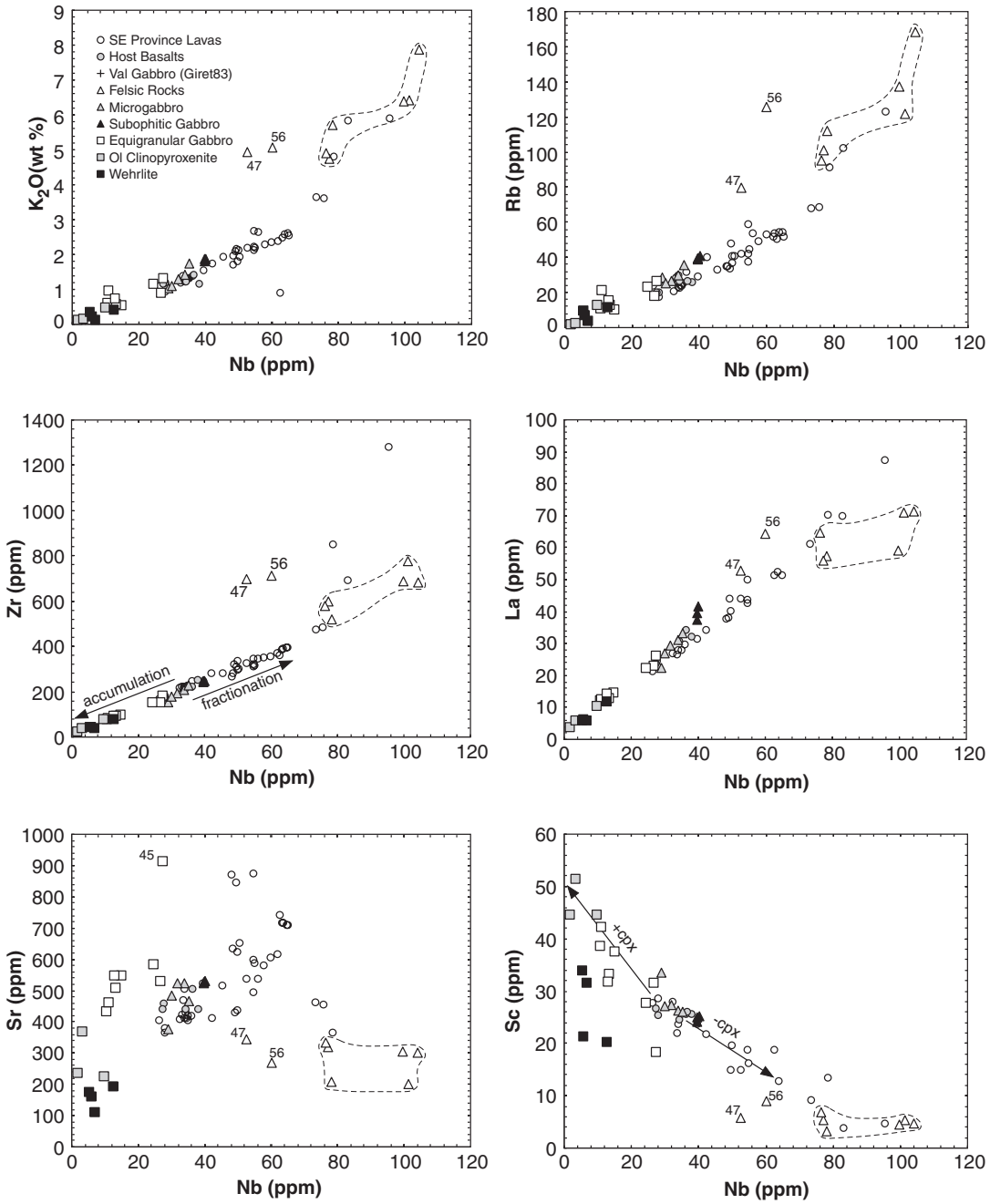

Fig. 8. K_2O (wt %), Rb, Zr, La, Sr and Sc vs Nb (ppm) diagrams for samples from the Val gabbro plutonic suite (this study) and volcanic rocks from the Southeast Province (Weis *et al.*, 1993; Frey *et al.*, 2000). Arrows in the Zr vs Nb panel show the relative effects of mineral accumulation and fractionation on incompatible element abundances. Arrows in the Sc vs Nb panel show trends associated with clinopyroxene accumulation (+ cpx) and fractionation (− cpx). The incompatible element-enriched felsic rocks are outlined by a dashed line (anomalous felsic rocks MPC99-47 and 56 are labeled).

of variable amounts of olivine, clinopyroxene and plagioclase from mildly alkalic parent magmas; (4) based on a relatively small range in Sr–Nd–Hf–Pb isotopic compositions, all rocks in the intrusion crystallized from a similar parent magma. Below we address differentiation processes and the source of parental magmas to the Val gabbro plutonic suite, and temporal changes in alkalinity in volcanic and plutonic rocks from the archipelago with implications for the existence of sub-volcanic magma chambers on the Kerguelen Archipelago.

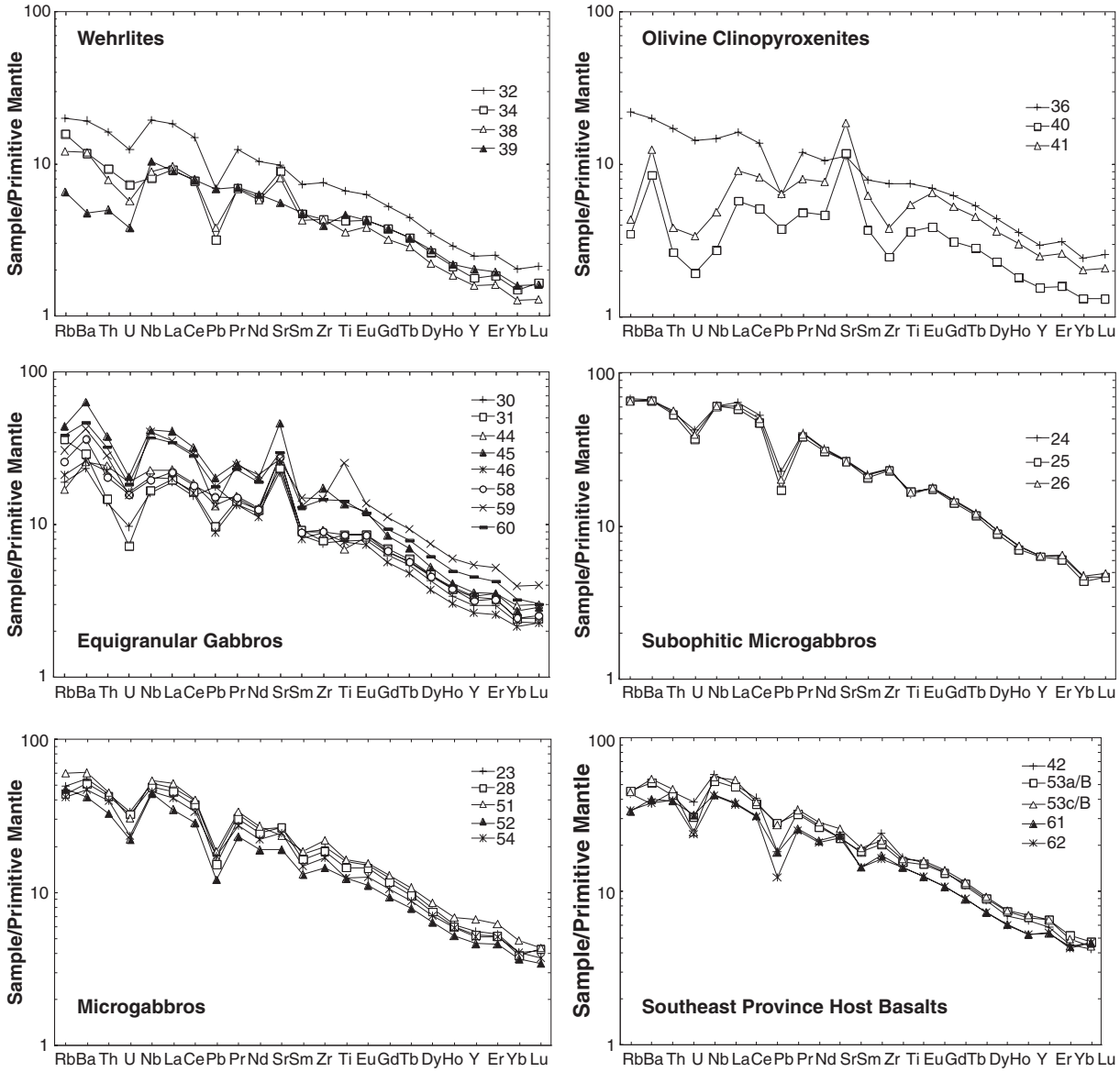

Fig. 9. Incompatible element abundances of samples from the Val gabbro plutonic suite (this study) and volcanic rocks from the Southeast Province (Frey *et al.*, 2000) normalized to the primitive mantle estimates of McDonough & Sun (1995).

Layering and crystal contents of magmas related to the Val gabbro plutonic suite

The Val gabbro plutonic suite is probably a relatively small exposure of a much larger intrusion; however, it provides a window into high-level differentiation processes in a volcanic oceanic island. The peridotites at the base of the cliff-face leading into the ocean (Fig. 2b) contain prominent macroscopic horizontal igneous layering, which can be observed from the cliffs above. Thus the deeper, unexposed levels of the Val gabbro plutonic suite may consist of a layered ultramafic intrusion, consistent with the positive Bouguer gravity anomaly that increases in magnitude towards the location of the intrusion in the SE part of the Jeanne d'Arc Peninsula (Recq & Charvis, 1986). Vertically layered gabbros, including the fine- to medium-grained equigranular gabbros and the coarse-grained plagioclase-bearing peridotites and melagabbros in this study, are up to 100 m thick in the vicinity of Cap du Challenger and extend for ~2000 m along the coastline to the NW (Fig. 2b). Vertical layering is not common in layered intrusions, but has been observed in bodies that represent solidified magma conduits (e.g. Falcon Lake intrusive complex, southeastern Manitoba, Canada; Mandziuk *et al.*, 1989). The presence in the Val gabbro plutonic suite of cumulate

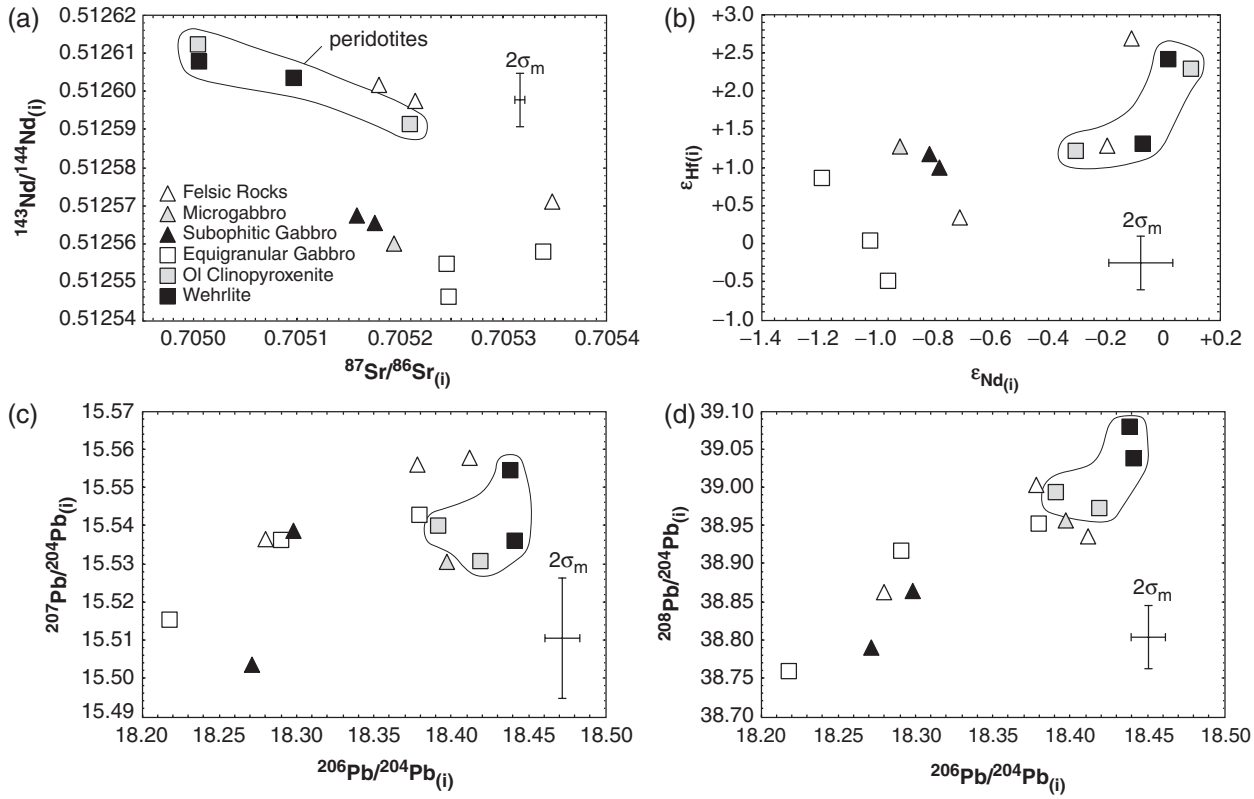

Fig. 10. Age-corrected (24 Ma) isotopic compositional variations of samples from the Val gabbro plutonic suite. (a) $^{143}Nd/^{144}Nd$ vs $^{87}Sr/^{86}Sr$, (b) ε_{Nd} vs ε_{Hf}, (c) $^{207}Pb/^{204}Pb$ vs $^{206}Pb/^{204}Pb$, (d) $^{208}Pb/^{204}Pb$ vs $^{206}Pb/^{204}Pb$ (subscript 'i' in figure indicates initial isotopic ratio). The errors bars for each diagram indicate the 2σ error of the measured ratios; the expanded scales for each of these diagrams relative to the analytical errors should be noted.

rocks with variable grain sizes, vertical modal layering, and prominent angular discontinuities suggests that they formed in response to repeated injections of magma with variable crystal contents along a fracture-controlled, sub-volcanic plumbing system during progressive dilation and contraction of the magma pathways (Giret & Beaux, 1984). Centimetre-scale modal layering in the equigranular gabbros may be related to these repeated pressure fluctuations; minor shifts in phase boundaries as a result of pressure changes in a magmatic system can produce large variations in the modal abundances of precipitating crystals (e.g. Naslund & McBirney, 1996).

The small grain size (millimetre-scale) of the layered equigranular gabbros is consistent with *in situ* formation of the cumulate rocks from injections of relatively crystal-poor to crystal-free magmas. In contrast, the large (>1 cm) olivine and clinopyroxene grains in the coarse-grained melagabbros to peridotites probably crystallized and grew at deeper levels below the current exposure of the intrusion. Based on olivine–melt equilibria (e.g. Roeder & Emslie, 1970), the most Fo-rich olivines observed in the peridotites ($Fo_{83–85}$; Fig. 5) indicate crystallization from magmas with ~8–10 wt % MgO. These crystals were transported upwards when ascent rates were sufficiently high to overcome the negative buoyant force exerted by the dense, centimetre-sized olivine and clinopyroxene, akin to the well-documented positive correlation between eruption flux and olivine phenocryst size and abundance in Hawaiian basalts (e.g. Murata & Richter, 1966). Few of the exposed volcanic rocks in the Southeast Province contain more than several modal per cent olivine and/or clinopyroxene phenocrysts (Weis *et al.*, 1993; Frey *et al.*, 2000) [notable exceptions are samples LVLK-70 and LVLK-88 of Weis *et al.* (1993)]. This suggests that large olivine and clinopyroxene crystals, such as those observed in the Val peridotites, were mostly trapped within sub-volcanic and deeper magma chambers and that they were extruded with lavas only during periods of locally increased magma flux or supply. Rare high-MgO basalts and picrites (6–17 wt % MgO) containing abundant (5–20 vol. %) olivine and clinopyroxene phenocrysts were erupted on the Kerguelen Archipelago (Doucet *et al.*, 2005, 2006); they have trace element and isotopic characteristics similar to those of the 24–25 Ma mildly alkalic basalts from the Southeast Province and Courbet Peninsula (Doucet *et al.*, 2005). Olivine core compositions in these high-MgO

basalts and picrites ($Fo_{74–87}$) overlap with those from the Val peridotites ($Fo_{68–86}$) and their respective clinopyroxene compositions are strikingly similar (Fig. 5), indicating that there may be a petrogenetic link between these two sample suites.

Compositional gap in mildly alkalic silica-oversaturated volcanic and plutonic rocks on the Kerguelen Archipelago

There is a notable compositional gap in basic and felsic rocks from the Val gabbro plutonic suite (from 49 to 58 wt % SiO_2) and a prominent, although smaller, compositional gap in volcanic rocks from the Southeast Province (from 52 to 56 wt % SiO_2) (Fig. 7). The existence of a compositional gap between the basic and felsic rocks on the Kerguelen Archipelago has been known since the original geological studies on the archipelago (LaCroix, 1924), mainly from the much younger Rallier-du-Baty ring complex on the southwestern part of the archipelago (Fig. 1), and was first referred to as a 'Daly gap' by Watkins *et al.* (1974). A Daly gap, or a bimodal distribution of basalt–rhyolite or alkali basalt–trachyte, occurs on many oceanic islands (e.g. Iceland, Ascension, Canary Islands) and a large number of proposals have been made to account for the missing intermediate members, including critical variations in physical properties such as viscosity and density (e.g. Schmincke, 1967; Jones, 1979; Geist *et al.*, 1995), large thermal and chemical changes produced by small changes in magma replenishment (e.g. Bonnefoi *et al.*, 1995), and remobilization of highly fractionated interstitial melt from the solidification front of crystallizing gabbros (solidification front instability) (Marsh, 1995). More recently, Freundt-Malecha *et al.* (2001) demonstrated that intermediate-composition plutonic fragments representing cumulate and melt compositions were erupted with composite rhyolitic–basaltic ignimbrites on Gran Canaria, a type locality for bimodal volcanism; thus it is clear that intermediate-composition magmas do form during fractional crystallization and are trapped in the conduit systems beneath some oceanic islands.

Are the felsic rocks in the Val gabbro plutonic suite related to the basic rocks by fractional crystallization? The Sr–Nd–Hf–Pb isotopic compositions of the analyzed felsic rocks (MPC99-47, 53a/A, 57) and microgabbro (MPC99-51) are similar (Fig. 10; Tables 3 and 4), which is permissive of such a relationship. Figure 7 shows fractional crystallization trends calculated with MELTS (Ghiorso & Sack, 1995) for a starting composition equivalent to a microgabbro (MPC99-54) under the following conditions: $fO_2 = FMQ - 1$ (where FMQ is the fayalite–magnetite–quartz buffer); starting water content is 0·75 wt % H_2O; pressure is 1, 5, and 9 kbar. The choice of oxygen fugacity and water content is based on the experimental results of Scoates *et al.* (2006) on the polybaric liquid-line-of-descent of mildly alkalic basalts on the Kerguelen Archipelago. The pressure range also corresponds to pressures used in the experiments of Scoates *et al.* (2006), which were based on the phenocryst crystallization environments identified by clinopyroxene–melt thermobarometry on mildly alkalic basalts from the Crozier section on the Courbet Peninsula by Damasceno *et al.* (2002). The MELTS trends for the three pressures in Fig. 7 terminate at 73–74% fractional crystallization and span the silica gap between the microgabbros and felsic rocks from the Val gabbro plutonic suite. The 1 kbar MELTS trend extends to higher SiO_2 contents than the higher-pressure trends, but underestimates alkali and Al_2O_3 contents compared with the higher-pressures trends (Fig. 7). The 5 kbar MELTS fractional crystallization trend provides the best fit to the observed geochemistry from the Val gabbro plutonic suite, which is consistent with the conclusion of Scoates *et al.* (2006) that high-pressure (>5 kbar) fractionation dominated by crystallization of high-Al clinopyroxene most closely reproduces the compositional variations of the 24–25 Ma mildly alkalic lavas on the Kerguelen Archipelago. The felsic rocks themselves are found as thin (<10 cm to 1 m), vertically oriented dikes that cut the basic rocks and overlying basaltic breccia (Fig. 2b). This suggests that they represent pathways for highly evolved melts, which is consistent with their formation by extensive fractionation deeper in the plumbing system below the exposed Val gabbro plutonic suite.

Where are the intermediate-composition lavas or plutonic rocks produced during fractional crystallization? Bimodal volcanism—trachytic flows and tuffs intercalated with trachybasalt—is preserved within the Ravin du Charbon and Jaune sections of the Jeanne d'Arc Peninsula (Fig. 2b; see Frey *et al.*, 2000, fig. 2). Bimodal volcanism is also characteristic of the youngest volcanic activity (26 ka) on the archipelago within the northern ring complex of the large Rallier-du-Baty volcano-plutonic complex (Gagnevin *et al.*, 2003). In contrast, there is a nearly continuous compositional trend from trachybasalt to trachyandesite in the 24–25 Ma Crozier section (Damasceno *et al.*, 2002; Scoates *et al.*, 2006, fig. 4) and from basaltic trachyandesite to trachyte erupted from the <1 Ma Mont Ross stratovolcano (Weis *et al.*, 1998). The compositions of plutonic rocks from the Rallier-du-Baty northern ring complex also fill the gap between the bimodal alkali basalt–trachyte lavas (Gagnevin *et al.*, 2003). Thus, the geological evidence indicates that under the appropriate conditions alkalic silica-oversaturated magmatism may produce either bimodal products or a continuum of compositions. It is possible that the Daly gap documented in the Val gabbro plutonic suite may simply be a function of the relatively small area of intrusive rocks actually exposed; additional exposures could potentially yield evolved dikes with intermediate compositions. However, given that the gap mimics that also recorded by the Southeast Province lavas and the

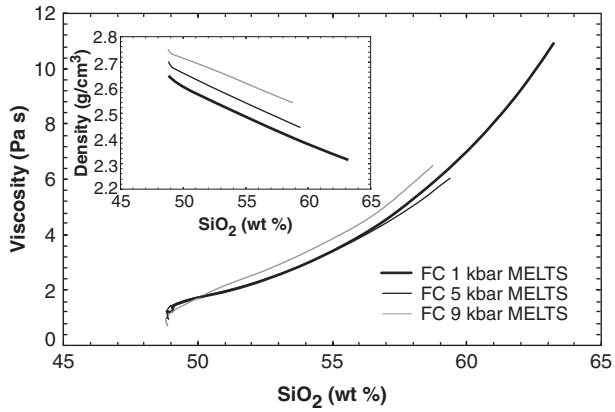

Fig. 11. Viscosity and density variations vs SiO_2 calculated using MELTS for evolved melts during fractional crystallization. The starting composition (microgabbro MPC99-54) and parameters (e.g. fO_2, H_2O, P) are the same as those indicated in Fig. 7. The observed Daly gap for samples from the Val gabbro plutonic suite is from 49 to 58 wt % SiO_2.

evidence for relatively high-pressure fractionation, the intermediate-composition magmas appear to have been trapped at depth during formation of volcanic rocks of the Southeast Province. Density–viscosity relations will have a major impact on the eruptibility of magmas (e.g. Marsh, 1981; Geist *et al.*, 1995). Using the MELTS results discussed above, the density of the evolved melts decreases progressively with fractionation (e.g. from 2·68 to 2·47 g/cm^3 at 5 kbar in the range of the observed silica gap from 49 to 58 wt % SiO_2, a decrease of ~8%; see inset in Fig. 11), which would favor buoyancy-driven flow. The viscosity of the evolved melts, however, increases substantially in the same interval, from 1·5 to 5·0 Pa s at 5 kbar (Fig. 11), thus helping to inhibit flow. Although other factors, such as magma crystallinity, will also play a role in restricting the upward flow of intermediate-composition magmas, the increased viscosity of evolved melts produced during fractionation at depth appears to be an important factor in the origin of a Daly gap in rocks from the Val gabbro plutonic suite. The fact that some intermediate-composition volcanic and plutonic rocks do occur elsewhere on the Kerguelen Archipelago indicates that other variables locally control eruptibility (e.g. vapor saturation).

Source of the parent magmas to the Val gabbro plutonic suite

The radiogenic isotopic compositions of samples from the Val gabbro plutonic suite are similar to those of the 24–25 Ma mildly alkalic basalts from the Kerguelen Archipelago (Fig. 12), including samples from the Southeast Province (Weis *et al.*, 1993; Frey *et al.*, 2000), the Crozier section on the Courbet Peninsula (Mattielli *et al.*, 2002; D. Weis, unpublished data), and high-MgO basalts and picrites that occur as cobbles in glacial moraines in the eastern part of the archipelago (Doucet *et al.*, 2005). These alkalic basalts are characterized by relatively low $^{87}Sr/^{86}Sr$ and high $^{143}Nd/^{144}Nd$, $^{176}Hf/^{177}Hf$ and Pb isotopic ratios compared with the 26–29 Ma tholeiitic–transitional basalts (Fig. 12). The tholeiitic–transitional basalts on the archipelago show clear evidence for mixing between a depleted mantle component, similar to that of Southeast Indian Ridge mid-ocean ridge basalt (MORB) (e.g. Yang *et al.*, 1998; Doucet *et al.*, 2002; Weis & Frey, 2002), and an enriched component characteristic of the Kerguelen mantle plume source (e.g. Mattielli *et al.*, 2002; Weis *et al.*, 2002; Ingle *et al.*, 2003). The magnitude of this depleted component in the Kerguelen Archipelago flood basalts decreased with decreasing age and increasing distance between the archipelago and the Southeast Indian Ridge as the ridge migrated to the NE relative to the nearly stationary Kerguelen hotspot (e.g. Gautier *et al.*, 1990; Weis *et al.*, 1993; Yang *et al.*, 1998; Doucet *et al.*, 2005). There is no contribution of the depleted mantle component in the source of the 24–25 Ma mildly alkalic basalts; these basalts were produced by melting of the enriched component of the Kerguelen plume source (Weis *et al.*, 1998; Frey *et al.*, 2000; Doucet *et al.*, 2005). Some of the samples from the Val gabbro plutonic suite (e.g. peridotites, felsic rocks, microgabbro) plot within the fields defined for the analyzed mildly alkalic basalts (Fig. 12), which is consistent with the major and trace element evidence that the parent magmas to the intrusion were part of the mildly alkalic silica-oversaturated series on the archipelago. However, the range of isotopic compositions for the Val gabbro plutonic suite extends to slightly higher $^{87}Sr/^{86}Sr$ and lower $^{143}Nd/^{144}Nd$, $^{176}Hf/^{177}Hf$ and Pb isotopic ratios than those defined by the Southeast Province and Crozier lavas, and their Pb isotopic compositions overlap those of the high-MgO basalts and picrites (Fig. 12). Based on Pb–Hf and Ne–He isotopic variations defined by the high-MgO basalts and picrites, Doucet *et al.* (2005, 2006) proposed that the Kerguelen mantle plume is characterized by the presence of dispersed compositional heterogeneities. Preferential sampling of one or more of these domains during melting and production of the parent magmas to the Val gabbro plutonic suite may explain the observed range of isotopic compositions defined by rocks from the intrusion.

Gabbroic sub-volcanic magma chambers at the end of flood basalt volcanism on the Kerguelen Archipelago

Recognition that the Val gabbro plutonic suite crystallized from mildly alkalic basaltic parental magmas and that the age of the intrusion is 24 Ma allows for a re-examination of the temporal relationship between volcanic and plutonic rocks on the Kerguelen Archipelago during flood basalt volcanism. Extensive glaciation and a regional southeasterly dip of the flood basalts of 2–5° exposes progressively

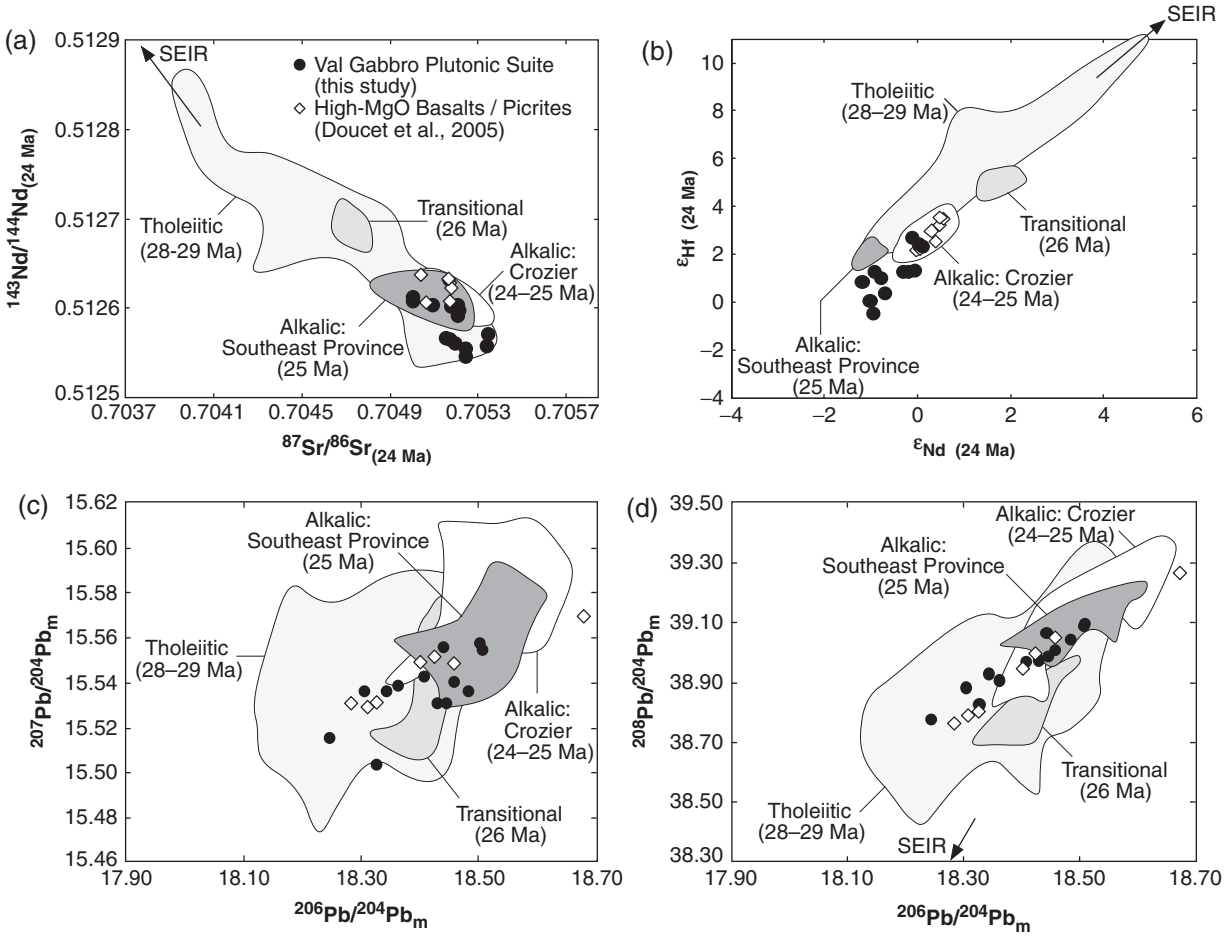

Fig. 12. Radiogenic isotopic compositions of samples from the Val gabbro plutonic suite compared with 24–29 Ma volcanic rocks from the Kerguelen Archipelago. (a) Initial $^{143}Nd/^{144}Nd$ vs initial $^{87}Sr/^{86}Sr$, (b) initial ε_{Nd} vs initial ε_{Hf}, (c) $^{207}Pb/^{204}Pb$ vs $^{206}Pb/^{204}Pb$, and (d) $^{208}Pb/^{204}Pb$ vs $^{206}Pb/^{204}Pb$ showing compositions for the Val gabbro plutonic suite (●), high-MgO basalts and picrites (◇), and volcanic rocks from the Kerguelen Archipelago (fields). The arrows point towards the composition of Southeast Indian Ridge (SEIR) MORB, which represents the depleted mantle reservoir. The isotopic composition of the 24–25 Ma Crozier basaltic section on the Kerguelen Archipelago, especially the radiogenic Pb isotopic composition, is considered to represent that of the 'enriched' component of the Kerguelen mantle plume (Mattielli *et al.*, 2002; Weis *et al.*, 2002). The 'tholeiitic basalts' field includes samples from the 28–29 Ma Bureau, Rabouillère, Ruches and Fontaine sections, and the 'transitional basalts' field includes samples from the 26 Ma Tourmente section. Data sources for the comparative isotopic geochemistry: Bureau and Rabouillère from Yang *et al.* (1998); Ruches and Fontaine from Doucet *et al.* (2002); Tourmente from Frey *et al.* (2002); Southeast Province from Weis *et al.* (1993) and Frey *et al.* (2000); Crozier from Mattielli *et al.* (2002) and D. Weis (unpublished data); high-MgO basalts and picrites from Doucet *et al.* (2005). The field for the Hf–Nd isotopic compositions of the Southeast Province samples is based on revised results (D. Weis, unpublished data) of the four samples originally published by Mattielli *et al.* (2002). All Pb isotopic data reported were measured by TIMS, except for the high-MgO basalt and picrites of Doucet *et al.* (2005), which were determined by MC-ICP-MS.

older and deeper sections to the NW across the Kerguelen Archipelago for the 26–29 Ma tholeiitic–transitional basalts; this corresponds to a 5–6 km stratigraphic section through the upper part of the archipelago based on an average 3° dip. There are no known contemporaneous high-level gabbroic intrusions exposed within these older basaltic sections. In contrast, the 24–25 Ma mildly alkalic basalts that cover the eastern part of the Kerguelen Archipelago (maximum exposed thickness of ~1000 m) are cut by a number of gabbroic intrusions that are interpreted to represent sub-volcanic intrusions to overlying (now-eroded) flows (e.g. Val and Gaby Island in the Southeast Province, and Montagnes Vertes on the Courbet Peninsula; Giret, 1983; this study). From 25 to 29 Ma, the average estimated lava accumulation rate is assumed to be constant at $1{\cdot}6 \pm 0{\cdot}9$ km/Myr and the average extrusive rate (magma supply or flux) over this same period was 0·009 km^3/year (Nicolaysen *et al.*, 2000). However, there is evidence for a decrease in eruption recurrence interval and magma supply in the 25 Ma volcanic rocks of the Southeast Province; the lower parts of the Ravin du Charbon and Jaune sections contain a

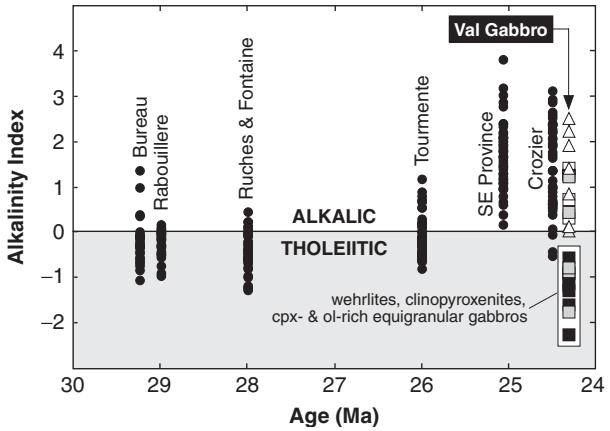

Fig. 13. Alkalinity index vs age for volcanic and plutonic rocks on the Kerguelen Archipelago between ~24 and 29 Ma. Alkalinity index $(AI) = (Na_2O + K_2O) - (0{\cdot}37SiO_2 - 14{\cdot}43)$ and is a measure of the distance of a given sample from the tholeiitic–alkalic boundary of MacDonald & Katsura (1964). Data sources for the geochemistry of the volcanic rocks: Bureau and Rabouillère from Yang *et al.* (1998); Ruches and Fontaine from Doucet *et al.* (2002); Tourmente from Frey *et al.* (2002); Southeast Province from Weis *et al.* (1993) and Frey *et al.* (2000); Crozier from D. Weis (unpublished data). Ages for the volcanic rocks are leached whole-rock or separated plagioclase $^{40}Ar/^{39}Ar$ dates from Frey *et al.* (2000), Doucet *et al.* (2002) and Nicolaysen *et al.* (2000), and the age of the Val gabbro plutonic suite is from this study (U–Pb zircon). The olivine- and clinopyroxene-rich peridotites from the Val gabbro plutonic suite are cumulate rocks that have accumulated low-alkali mafic minerals, thus their bulk compositions lie within the tholeiitic field.

conglomerate unit (40–70 m thick) with clasts of basalt and trachyte and discrete lignite horizons (Leyrit, 1992; Frey *et al.*, 2000). Thus, the emplacement of high-level gabbroic intrusions occurred at the very end of flood basalt volcanism on the Kerguelen Archipelago as magma supply appeared to be waning.

The presence of sub-volcanic gabbroic intrusions also follows a distinct increase in the alkalinity of the erupted basalts (Fig. 13), which suggests a link with variations in melting history for basalts on the Kerguelen Archipelago. The first systematic appearance of alkalic basalts (alkalinity index >0) occurs within the upper 100 m of the Tourmente section (Frey *et al.*, 2002) (see location in Fig. 1). The Tourmente magmas segregated within the stability field of spinel peridotite, with the uppermost alkalic lavas representing lower degrees of melting and segregation at higher pressures than the transitional lavas in the lower part of the section (Frey *et al.*, 2002). The chemistry of the 25 Ma mildly alkalic lavas in the Southeast Province also indicates decreased extents of melting compared with the tholeiitic–transitional basalts on the archipelago, but also increased pressures of segregation within the garnet stability field (Frey *et al.*, 2000) and a significant role for fractionation of high-Al clinopyroxene at pressures corresponding to the crust–mantle transition zone beneath the archipelago (14–16 km) (Damasceno *et al.*, 2002; Scoates *et al.*, 2006). This change in basalt chemistry is primarily a function of thickening of the cooling lithosphere as the distance between the Northern Kerguelen Plateau and Southeast Indian Ridge increased during the period from ~40 Ma to 25 Ma (i.e. from a ridge-centred setting to a distance of 400 km) (Frey *et al.*, 2000; Scoates *et al.*, 2006), which forced decompression melting within the Kerguelen mantle plume to progressively deeper levels. Following eruption of the exposed 24–25 Ma mildly alkalic basalts, sub-volcanic gabbroic intrusions such as the Val gabbro plutonic suite were emplaced, and signal the end of flood basalt magmatism on the Kerguelen Archipelago as volcanism related to the Kerguelen plume shifted location several hundred kilometres to the SE beneath the Central Kerguelen Plateau (Weis *et al.*, 2002).

CONCLUSIONS

This study of the Val gabbro plutonic suite in the Southeast Province of the Kerguelen Archipelago, a major oceanic island in the Southern Indian Ocean, provides constraints on the relationship between high-level sub-volcanic magma reservoirs and flood basalt volcanism. The intrusion consists principally of vertically layered mafic–ultramafic rocks that overlie horizontally layered peridotites with local fine-grained marginal gabbros and rare cross-cutting felsic dikes (monzonite to quartz monzonite). A precise U–Pb zircon age of 24·25 ± 0·15 Ma for a subophitic microgabbro is interpreted as the age of crystallization of the intrusion, which indicates that the Val gabbro plutonic suite is only slightly younger than the hosting 25 Ma mildly alkalic basalts of the Southeast Province. Strong major and trace element and Sr–Nd–Hf–Pb isotopic compositional similarities between the fine-grained marginal gabbros and cross-cutting felsic rocks with the Southeast Province volcanic rocks (basalts and trachytes) indicate that the parental magmas to the plutonic rocks belong to the mildly alkalic silica-oversaturated magma series on the archipelago. The petrological and geochemical variations of the vertically layered cumulate rocks (plagioclase-bearing peridotites–olivine melagabbros and equigranular gabbros) are consistent with those produced by injections of mildly alkalic basaltic magmas with variable crystallinity into a sub-volcanic magma plumbing system during repeated dilation and contraction of the magma pathways. Differentiated, sub-volcanic gabbroic intrusions such as the Val gabbro plutonic suite do not occur within the older 26–29 Ma transitional basalts on the Kerguelen Archipelago, but were emplaced only when volcanism on the archipelago changed to mildly alkalic compositions after 25 Ma. This increase in alkalinity is also associated with evidence for lower extents of melting, deeper melting, a change in source components towards a plume-dominated

enriched composition, and the presence of discrete volcanic hiatuses within volcanic rocks of the Southeast Province. The emplacement and crystallization of the Val gabbro plutonic suite at 24 Ma signals the end of flood basalt volcanism on the Kerguelen Archipelago.

ACKNOWLEDGEMENTS

We are greatly indebted to the IFRTP (Institut Français pour la Recherche et la Technologie Polaire), now IPEV (Institut Polaire Français Paul Emile Victor), and the captains and crew of the *Marion Dufresne II* and the *Curieuse* for their critical support of fieldwork on the Kerguelen Archipelago. We are grateful to Gilbert Michon, W. Powell, and Jean-Yves Cottin for diligently undertaking the new sampling of the Val gabbro plutonic suite in February 1999 in an area where access is difficult. The microprobe analyses were carried out under the always capable supervision of Mati Raudsepp at the University of British Columbia. Many thanks go to Jim Mortensen and Rich Friedman at UBC for the careful U–Pb analyses of zircon and baddeleyite. The ICP-MS trace element analyses at the University of Göteborg, Sweden, would not have been possible without the guidance and patience of Bill Meurer. Edouard Foriers carried out the Hf isotope chemistry and Claude Maerschalk provided important assistance during all of the chemical preparation stages of samples for Sr–Nd–Hf–Pb isotopic work at the Université Libre de Bruxelles. Discussions with Mauro Lo Cascio concerning his experimental work on mildly alkalic basalts from the Kerguelen Archipelago were extremely useful. Reviews by Armin Freundt and an anonymous reviewer plus editorial comments by Colin Devey helped to improve the clarity of the final manuscript. This research was supported with funding to Scoates, Weis, and Mattielli from the Communauté Française of Belgium (Actions de Recherche Concertées ARC Convention 98/03-233), to Frey from US NSF Grant EAR9814313, and to Scoates and Weis by Canadian NSERC Discovery Grants.

SUPPLEMENTARY DATA

Supplementary data for this paper are available at *Journal of Petrology* online.

REFERENCES

Beaux, J. F. (1986). Le complexe volcano-plutonique de la Presqu'île de la Société de Géographie (Iles Kerguelen). Structure et pétrologie. Ph.D. thesis, Université Pierre et Marie Curie, Paris, 203 pp.

Blichert-Toft, J., Chauvel, C. & Albarède, F. (1997). Separation of Hf and Lu for high-precision isotope analysis of rock samples by magnetic sector-multiple collector ICP-MS. *Contributions to Mineralogy and Petrology* **127**, 248–260.

Bonnefoi, C. C., Provost, A. & Albarède, F. (1995). The 'Daly gap' as a magmatic catastrophe. *Nature* **378**, 270–272.

Chauvel, C. & Blichert-Toft, J. (2001). A hafnium isotope and trace element perspective on melting of the depleted mantle. *Earth and Planetary Science Letters* **190**, 137–151.

Damasceno, D., Scoates, J. S., Weis, D., Frey, F. A. & Giret, A. (2002). Mineral chemistry of mildly alkalic basalts from the 25 Ma Mont Crozier section, Kerguelen Archipelago: constraints on phenocryst crystallization environments. *Journal of Petrology* **43**, 1389–1413.

Dosso, L., Vidal, P., Cantagrel, J.-M., Lameyre, J., Marot, A. & Zimine, S. (1979). 'Kerguelen: continental fragment or oceanic island?'; petrology and isotopic geochemistry evidence. *Earth and Planetary Science Letters* **43**, 46–60.

Doucet, S., Weis, D., Scoates, J. S., Nicolaysen, K., Frey, F. A. & Giret, A. (2002). The depleted mantle component in Kerguelen Archipelago basalts: petrogenesis of tholeiitic–transitional basalts from the Loranchet Peninsula. *Journal of Petrology* **43**, 1341–1366.

Doucet, S., Scoates, J. S., Weis, D. & Giret, A. (2005). Constraining the components of the Kerguelen mantle plume: a Hf–Pb–Sr–Nd isotopic study of picrites and high-MgO basalts from the Kerguelen Archipelago. *Geochemistry, Geophysics, Geosystems*, doi:10.1029/2004GC000806.

Doucet, S., Moreira, M., Weis, D., Scoates, J. S., Giret, A. & Allègre, C. (2006). Primitive neon and helium isotopic compositions of high-MgO basalts from the Kerguelen Archipelago, Indian Ocean. *Earth and Planetary Science Letters* **241**, 65–79.

Freundt-Malecha, B., Schmincke, H.-U. & Freundt, A. (2001). Plutonic rocks of intermediate composition on Gran Canaria: the missing link of the bimodal volcanic rock suite. *Contributions to Mineralogy and Petrology* **141**, 430–445.

Frey, F. A., Weis, D., Yang, H. J., Nicolaysen, K., Leyrit, H. & Giret, A. (2000). Temporal geochemical trends in the Kerguelen archipelago basalts: evidence for decreasing magma supply from the Kerguelen plume. *Chemical Geology* **164**, 61–80.

Frey, F. A., Nicolaysen, K. A., Kubit, B. K., Weis, D. & Giret, A. (2002). Flood basalts from Mont Tourmente in the central Kerguelen Archipelago: the change from tholeiitic/transitional to alkali basalts at ~25 Ma. *Journal of Petrology* **43**, 1367–1387.

Gagnevin, D., Ethien, R., Bonin, B., Moine, B., Féraud, G., Gerbe, M. C., Cottin, J. Y., Michon, G., Tourpin, S., Mamias, G., Perrache, C. & Giret, A. (2003). Open-system processes in the genesis of silica-oversaturated alkaline rocks of the Rallier-du-Baty Peninsula, Kerguelen Archipelago (Indian Ocean). *Journal of Volcanology and Geothermal Research* **123**, 267–300.

Gautier, I., Weis, D., Mennessier, J.-P., Vidal, P., Giret, A. & Loubet, M. (1990). Petrology and geochemistry of Kerguelen basalts (South Indian Ocean): evolution of the mantle sources from ridge to an intraplate position. *Earth and Planetary Science Letters* **100**, 59–76.

Geist, D., Howard, K. A. & Larson, P. (1995). The generation of oceanic rhyolites by crystal fractionation: the basalt–rhyolite association at Volcan Alcedo, Galapagos Archipelago. *Journal of Petrology* **36**, 965–982.

Ghiorso, M. S. & Sack, R. O. (1995). Chemical mass transfer in magmatic processes IV. A revised and internally consistent thermodynamic model for the interpolation and extrapolation of liquid–solid equilibria in magmatic systems at elevated temperatures and pressures. *Contributions to Mineralogy and Petrology* **119**, 197–212.

Giret, A. (1983). Le plutonisme océanique intraplaque, exemple de l'archipel Kerguelen. Thèse doctorat d'Etat, Université Pierre et Marie Curie, Paris, 290 pp.

Giret, A. & Beaux, J.-F. (1984). Le pluton du Val Gabbro (îles Kerguelen), un complexe tholéiitique témoin de l'activité de la

paléo-ride Est-Indienne. *Comptes Rendus de l'Académie des Sciences* **299**, 965–970.

Giret, A. & Lameyre, J. (1984). A study of Kerguelen plutonism: petrology, geochronology and geological implications. In: Oliver, R. L., James, P. R. & Jago, J. B. (eds) *Antarctic Earth Science: Fourth International Symposium*. Cambridge: Cambridge University Press, pp. 646–651.

Giret, A., Bonin, B. & Léger, J. M. (1980). Amphibole compositional trends in oversaturated and undersaturated alkaline plutonic ring complexes. *Canadian Mineralogist* **18**, 481–495.

Giret, A., Cantagrel, J. M. & Nougier, J. (1981). Nouvelles données sur les complexes volcano-plutoniques des îles Kerguelen. *Comptes Rendus de l'Académie des Sciences* **306**, 381–386.

Goolaerts, A., Mattielli, N., de Jong, J., Weis, D. & Scoates, J. S. (2004). Hf and Lu isotopic reference values for the zircon standard 91500 by MC-ICP-MS. *Chemical Geology* **206**, 1–9.

Gradstein, F., Ogg, J. & Smith, A. (2004). *A Geologic Time Scale*. Cambridge University Press, Cambridge, 589 pp.

Ingle, S., Weis, D., Doucet, D. & Mattielli, N. (2003). Hf isotope constraints on mantle sources and shallow-level contaminants during Kerguelen hot spot activity since ~120 Ma. *Geochemistry, Geophysics, Geosystems*, doi:10.1029/2002GC000482.

Jang, Y. D. & Naslund, H. R. (2003). Major and trace element variation in ilmenite in the Skaergaard intrusion: petrologic implications. *Chemical Geology* **193**, 109–125.

Jones, W. B. (1979). Mixed benmoreite/trachyte flows from Kenya and their bearing on the Daly gap. *Geological Magazine* **116**, 487–489.

LaCroix, A. (1924). Les roches éruptives grenues de l'archipel de Kerguelen. *Comptes Rendus de l'Académie des Sciences* **179**, 113–119.

Lameyre, J., Marot, A., Zimine, S., Cantagrel, J.-M., Dosso, L. & Vidal, P. (1976). Chronological evolution of the Kerguelen islands syenite–granite ring complex. *Nature* **263**, 306–307.

Leyrit, H. (1992). Kerguelen: cartographie et magmatologie des presqu'îles Jeanne d'Arc et Ronarc'h. Ph.D. thesis, Université Paris-Sud, 236 pp.

MacDonald, G. A. & Katsura, T. (1964). Chemical composition of Hawaiian lavas. *Journal of Petrology* **5**, 82–133.

Mandziuk, W. S., Brisbin, W. C. & Scoates, R. F. J. (1989). Igneous structures in the Falcon Lake intrusive complex, southeastern Manitoba. *Canadian Mineralogist* **27**, 81–92.

Marot, A. & Zimine, S. (1976). Les complexes annulaires de syénites et granites alcalins dans la péninsule Rallier du Baty. Iles Kerguelen (TAAF). Ph.D. thesis, Université Pierre et Marie Curie, Paris.

Marsh, B. D. (1981). On the crystallinity, probability of occurrence, and rheology of lava and magma. *Contributions to Mineralogy and Petrology* **78**, 85–98.

Marsh, B. D. (1995). Solidification fronts and magmatic evolution. *Mineralogical Magazine* **60**, 5–40.

Mattielli, N., Weis, D., Blichert-Toft, J. & Albarède, F. (2002). Hf isotopic evidence for a Miocene change in the Kerguelen mantle plume composition. *Journal of Petrology* **43**, 1327–1339.

McDonough, W. F. & Sun, S.-s. (1995). The composition of the Earth. *Chemical Geology* **120**, 223–253.

McKay, G. A. (1989). Partitioning of rare earth elements between major silicate minerals and basaltic melts. In: Lipin, B. R. & McKay, G. A. (eds) *Geochemistry and Mineralogy of Rare Earth Elements. Mineralogical Society of America, Reviews in Mineralogy* **21**, 45–77.

Mortensen, J. K., Ghosh, D. & Ferri, F. (1995). U–Pb age constraints of intrusive rocks associated with copper–gold porphyry deposits in the Canadian Cordillera. In: Schroeter, T. G. (ed.) *Porphyry Deposits of the Northwestern Cordillera of North America. Canadian Institute of Mining and Metallurgy, Special Volume* **46**, 142–158.

Murata, K. J. & Richter, D. H. (1966). The settling of olivine in Kilauean magma as shown by lavas of the 1959 eruption. *American Journal of Science* **264**, 194–203.

Naslund, H. R. & McBirney, A. R. (1996). Mechanisms of formation of igneous layering. In: Cawthorn, E. G. (ed.) *Layered Intrusions*. Amsterdam: Elsevier, pp. 1–43.

Nicolaysen, K., Frey, F. A., Hodges, K. V., Weis, D. & Giret, A. (2000). $^{40}Ar/^{39}Ar$ geochronology of flood basalts from the Kerguelen Archipelago, southern Indian Ocean: implications for Cenozoic eruption rates of the Kerguelen plume. *Earth and Planetary Science Letters* **174**, 313–328.

Nougier, J. (1970). *Contribution à l'étude géologique et géomorphologique des îles Kerguelen (Terres Australes et Antarctiques Françaises): Tomes I et II. Bulletin CNFRA*. Paris: TAAF, 440 ppand 246 pp.

Nougier, J. & Lameyre, J. (1973). Les normarkites des îles Kerguelen (TAAF) dans leur cadre structural: problème de leur origine et de celle de certaines roches plutoniques alcalines en domaines océaniques. *Bulletin de la Société Géologique de France* **7**, 306–311.

Nougier, J., Pawlowski, D. & Cantagrel, J. M. (1984). Chrono-spatial evolution of the volcanic activity in southeastern Kerguelen (TAAF). In: Oliver, R. L., James, P. R. & Jago, J. B. (eds) *Antarctic Earth Science: Fourth International Symposium*. Cambridge: Cambridge University Press, pp. 640–645.

Pouchou, J. L. & Pichoir, F. (1991). Quantitative analysis of homogeneous or stratified microvolumes applying the model 'PAP'. In: Heinrich, K. F. J. & Newbury, D. E. (eds) *Electron Probe Quantitation*. New York: Plenum, pp. 31–75.

Recq, M. & Charvis, P. (1986). A seismic refraction survey in the Kerguelen Isles, southern Indian Ocean. *Geophysical Journal of the Royal Astronomical Society* **84**, 529–559.

Rhodes, J. M. (1996). Geochemical stratigraphy of lava flows sampled by the Hawaii Scientific Drilling Project. *Journal of Geophysical Research* **101**, 11729–11746.

Rhodes, J. M. & Vollinger, M. J. (2004). Composition of basaltic lavas sampled by phase-2 of the Hawaii Scientific Drilling Project: geochemical stratigraphy and magma types. *Geochemistry, Geophysics, Geosystems*, doi:10.1029/2002GC000434.

Roddick, J. C. (1987). Generalized numerical error analysis with application to geochronology and thermodynamics. *Geochimica et Cosmochimica Acta* **51**, 2129–2135.

Roeder, P. L. & Emslie, R. F. (1970). Olivine–liquid equilibrium. *Contributions to Mineralogy and Petrology* **29**, 275–289.

Rosman, J. R. & Taylor, P. D. P. (1998). Isotopic compositions of the elements. *Pure and Applied Chemistry* **70**, 217–236.

Schmincke, H.-U. (1967). Cone sheet swarm, resurgence of Tejeda Caldera, and the early history of Gran Canaria. *Bulletin of Volcanology* **31**, 153–162.

Scoates, J. S., Lo Cascio, M., Weis, D. & Lindsley, D. H. (2006). Experimental constraints on the origin and evolution of mildly alkalic basalts from the Kerguelen Archipelago, Southeast Indian Ocean. *Contributions to Mineralogy and Petrology* **151**, 582–599.

Stacey, J. S. & Kramer, J. D. (1975). Approximation of terrestrial lead isotope evolution by a two-stage model. *Earth and Planetary Science Letters* **26**, 207–221.

Steiger, R. H. & Jäger, E. (1977). Subcommission on geochronology: convention on the use of decay constants in geo- and cosmochronology. *Earth and Planetary Science Letters* **36**, 359–362.

Watkins, N. D., Gunn, B. M., Nougier, J. & Baksi, A. K. (1974). Kerguelen: continental fragment or oceanic island? *Geological Society of America Bulletin* **85**, 201–212.

Weis, D. & Frey, F. A. (2002). ODP Site 1140 on the Northern Kerguelen Plateau: 34 Ma pillow basalts related to the Kerguelen plume and the Southeast Indian Ridge. *Journal of Petrology* **43**, 1287–1309.

Weis, D. & Giret, A. (1994). Kerguelen plutonic complexes: Sr, Nd, Pb isotopic study and inferences about their sources age and geodynamic setting. *Mémoires de la Société Géologique de la France* **166**, 47–59.

Weis, D., Demaiffe, D., Cauët, S. & Javoy, M. (1987). Sr, Nd, O and H isotopic ratios in Ascension lavas and plutonic inclusions: cogenetic origin. *Earth and Planetary Science Letters* **82**, 316–322.

Weis, D., Frey, F. A., Leyrit, H. & Gautier, I. (1993). Kerguelen Archipelago revisited: geochemical and isotopic study of the Southeast Province lavas. *Earth and Planetary Science Letters* **118**, 101–119.

Weis, D., Frey, F. A., Giret, A. & Cantagrel, J.-M. (1998). Geochemical characteristics of the youngest volcano (Mount Ross) in the Kerguelen Archipelago: inferences for magma flux, lithosphere assimilation and composition of the Kerguelen plume. *Journal of Petrology* **39**, 973–994.

Weis, D., Frey, F. A., Schlich, R., Schaming, M., Montigny, R., Damasceno, D., Mattielli, N., Nicolaysen, K. E. & Scoates, J. S. (2002). Trace of the Kerguelen mantle plume: evidence from seamounts between the Kerguelen Archipelago and Heard Island, Indian Ocean. *Geochemistry, Geophysics, Geosystems*, doi:10.1029/2001GC000251.

Weis, D., Kieffer, B., Maerschalk, C., Barling, J., de Jong, J., Williams, G. A., Hanano, D., Pretorius, W., Mattielli, N., Scoates, J. S., Goolaerts, A., Friedman, R. M. & Mahoney, J. B. (2006). High-precision isotopic characterization of USGS reference materials by TIMS and MC-ICP-MS. *Geochemistry, Geophysics, Geosystems*, doi:10.1029/2006GC001283.

Weis, D., Kieffer, B., Hanano, D., Nobre Silva, I, Barling, J., Pretorius, W., Maerschalk, C. & Mattielli, N. (2007). Hf isotope compositions of US Geological Survey reference materials. *Geochemistry, Geophysics, Geosystems*, doi:10.1029/2006GC001473.

Yang, H.-J., Frey, F. A., Weis, D., Giret, A., Pyle, D. & Michon, G. (1998). Petrogenesis of the flood basalts forming the northern Kerguelen Archipelago: implications for the Kerguelen plume. *Journal of Petrology* **39**, 711–748.

APPENDIX: LOCATIONS OF GEOCHEMICAL SAMPLES FROM THE VAL GABBRO PLUTONIC SUITE

Sample no.	Rock type	Latitude	Longitude
MPC99-32	Wehrlite	−49·711446	70·080074
MPC99-34	Wehrlite	−49·711446	70·080074
MPC99-38	Wehrlite	−49·711446	70·080074
MPC99-39	Wehrlite	−49·711446	70·080074
MPC99-36	Olivine clinopyroxenite	−49·711446	70·080074
MPC99-40	Olivine clinopyroxenite	−49·724819	70·080742
MPC99-41	Olivine clinopyroxenite	−49·724819	70·080742
MPC99-30	Equigranular gabbro	−49·711446	70·080074
MPC99-31	Equigranular gabbro	−49·711446	70·080074
MPC99-44	Equigranular gabbro	−49·726303	70·081878
MPC99-45	Equigranular gabbro	−49·726303	70·081878
MPC99-46	Equigranular gabbro	−49·729124	70·075181
MPC99-58	Equigranular gabbro	−49·716361	70·077749
MPC99-59	Equigranular gabbro	−49·716361	70·077749
MPC99-60	Equigranular gabbro	−49·716361	70·077749
MPC99-23	Microgabbro	−49·710217	70·079229
MPC99-28	Microgabbro	−49·710217	70·079229
MPC99-51	Microgabbro	−49·720670	70·075240
MPC99-52	Microgabbro	−49·720670	70·075240
MPC99-54	Microgabbro	−49·719004	70·074775
MPC99-24	Subophitic microgabbro	−49·710217	70·079229
MPC99-25	Subophitic microgabbro	−49·710217	70·079229
MPC99-26	Subophitic microgabbro	−49·710217	70·079229
MPC99-47	Felsic rock	−49·727636	70·072805
MPC99-49	Felsic rock	−49·727636	70·072805
MPC99-50	Felsic rock	−49·720670	70·075240
MPC99-53a/A	Felsic rock	−49·719004	70·074775
MPC99-53b/A	Felsic rock	−49·719004	70·074775
MPC99-53c/A	Felsic rock	−49·719004	70·074775
MPC99-56	Felsic rock	−49·716361	70·077749
MPC99-57	Felsic rock	−49·716361	70·077749
MPC99-42	Basalt	−49·727602	70·083015
MPC99-53a/B	Basalt	−49·719004	70·074775
MPC99-53c/B	Basalt	−49·719004	70·074775
MPC99-61	Basalt	−49·695745	70·120294
MPC99-62	Basalt	−49·695745	70·120294

Sample locations (latitudes and longitudes are given as decimal degrees) referenced from GoogleEarth, version 4.0.2093 (beta).